Research Square

Preprints are preliminary reports that have not undergone peer review.
They should not be considered conclusive, used to inform clinical practice,
or referenced by the media as validated information.

Targeting the LIPH-CD36 axis potentiates CDK4/6 inhibition in ER+ breast cancer

Andrea Morandi

andrea.morandi@unifi.it

University of Florence https://orcid.org/0000-0002-9222-5332

Nicla Lorito

University of Florence

Elisabetta Romano

University of Florence

Alfredo Smiriglia

University of Florence

Marina Bacci

University of Florence https://orcid.org/0000-0001-8506-2179

Francesca Bonechi

University of Florence

Martín González-Fernández

Edoardo Pagliantini

Gabriele Tani

Giuseppina Comito

Bruno Simões

Manchester Breast Centre, Division of Cancer Sciences, Faculty of Biology, Medicine and Health, University of Manchester https://orcid.org/0000-0003-1253-6657

Robert Clarke

Manchester Breast Centre, Division of Cancer Sciences, Faculty of Biology, Medicine and Health, University of Manchester https://orcid.org/0000-0001-5407-3123

Rania El-botty

Laura Sourd

Icro Meattini

Luca Visani

Simonetta Bianchi

Lorenzo Livi

Elisabetta Marangoni

Translational Research Department, Institut Curie https://orcid.org/0000-0002-3337-6448

Sven Rottenberg

University of Bern https://orcid.org/0000-0003-2044-9844

Paola Francica

University of Bern https://orcid.org/0009-0005-4988-5940

Article

Keywords: lipid signaling, therapy resistance, estrogens, endocrine therapy, metabolism

Posted Date: August 7th, 2026

DOI: https://doi.org/10.21203/rs.3.rs-10541704/v1

License: This work is licensed under a Creative Commons Attribution 4.0 International License.
Read Full License

Additional Declarations: Yes there is potential conflict of interest.

Abstract

ER+/HER2 − breast cancer is commonly treated with endocrine therapy combined with CDK4/6 inhibitors (CDK4/6i), including palbociclib, ribociclib, and abemaciclib. Although these combinations have improved clinical outcome, resistance remains frequent, highlighting the need to identify vulnerabilities that enhance CDK4/6i response.

To uncover metabolic dependencies associated with CDK4/6i sensitivity, we performed an unbiased loss-of-function screen targeting ~2,800 metabolic genes. This identified lipase H (LIPH), a phosphatidic acid-selective phospholipase A1 that generates lysophosphatidic acid (LPA), as a candidate vulnerability in palbociclib-treated ER+/HER2- breast cancer cells. LIPH depletion reduced LPA levels and sensitized multiple ER+ models to palbociclib, ribociclib, and abemaciclib. Mechanistically, LIPH-derived LPA activated LPAR2-dependent AMPK/p38 signaling, sustaining CD36 expression. CD36 regulated cyclin D1 levels and cell-cycle progression, while LIPH or CD36 depletion reduced cyclin D1, induced G0/G1 accumulation, and enhanced CDK4/6i sensitivity. Conversely, exogenous LPA restored CD36 and cyclin D1 expression in LIPH-silenced cells. Genetic or pharmacological CD36 targeting potentiated CDK4/6i efficacy in endocrine-sensitive and therapy-resistant ER+ models, as well as in patient-derived organoids.

Clinically, high LIPH/CD36 scores were associated with poor response to CDK4/6i-based therapy, while elevated LIPH, CD36, or combined LIPH/LPAR2/CD36 expression correlated with worse outcome in ER+/HER2 − breast cancer cohorts. Together, our findings identify the LIPH–LPA–LPAR2–CD36–cyclin D1 axis as a lipid-signaling vulnerability that modulates CDK4/6i response and propose LIPH and CD36 as candidate therapeutic targets and biomarkers in ER+/HER2- breast cancer.

Introduction

The addition of cyclin-dependent kinase 4 and 6 inhibitors (CDK4/6i), namely palbociclib, ribociclib, and abemaciclib, to endocrine therapy has become a standard-of-care treatment for advanced and high-risk estrogen receptor-positive (ER+) and human epidermal growth factor receptor 2-negative (HER2-) breast cancer[1]. Despite the substantial improvement in progression-free survival (PFS) and overall survival (OS) achieved in this disease setting, many patients ultimately relapse with therapy-resistant disease[2], underscoring the need for novel strategies to enhance sensitivity, delay the emergence of resistance, and ideally restore responsiveness to CDK4/6i-based therapy.

Most preclinical studies have identified alterations in canonical cell-cycle regulators, including retinoblastoma protein (RB, encoded by *RB1*), cyclin E (encoded by *CCNE*), and aurora kinase A (encoded by *AURKA*), as well as oncogenic signaling pathways, such as phosphoinositide 3-kinase (PI3K)/protein kinase B (AKT)/mechanistic target of rapamycin (mTOR) and Kirsten rat sarcoma viral oncogene homolog (KRAS), as determinants of CDK4/6i resistance[3]. These mechanisms have also been confirmed in clinical samples[4]. However, CDK4/6 proteins have increasingly been recognized to exert non-canonical functions beyond cell-cycle control, including roles in cellular metabolism[5–7]. In line with this, CDK4/6i

have been shown to directly reprogram anabolic and catabolic pathways[8,9]. Crucially, we and others have shown that CDK4/6i resistance is characterized by profound metabolic rewiring, revealing potentially actionable metabolic vulnerabilities[10–14].

Within this metabolic framework, lipid remodeling is particularly relevant because bioactive lipid mediators can simultaneously influence tumor cell proliferation, survival, migration, immune interactions, and therapeutic adaptation[15,16]. Lipase H (LIPH, also known as phosphatidic acid-selective phospholipase A1) hydrolyzes phosphatidic acid (PA) to generate 2-acyl lysophosphatidic acid (LPA), a potent bioactive lipid mediator[17]. LPA potentially signals through six different G-protein-coupled LPA receptors (LPARs) and has been implicated in tumor progression and therapy resistance across different cancer types[18,19], including breast cancer[20,21]. In breast tumor models, the LPA-induced LPAR downstream activation has been linked to proliferative and migratory phenotypes, while pharmacologic inhibition of LPA-LPAR signaling can attenuate these tumor-associated behaviors[22]. These observations suggest that lipid metabolic pathways may offer previously underexplored determinants of CDK4/6i response and resistance.

To identify these vulnerabilities, we performed an unbiased loss-of-function dropout screen targeting metabolism-related genes in ER+/HER2- breast cancer cells treated with CDK4/6i, and we identified LIPH as a candidate metabolic vulnerability. Subsequent mechanistic validation revealed that LIPH-dependent LPA production sustains a downstream LPAR2–AMPK/p38–CD36–CCND1 signaling axis that modulates CDK4/6i sensitivity. These targets were orthogonally validated using cell lines, patient-derived organoids (PDOs) and clinical samples, supporting the LIPH-CD36 axis as a promising strategy to delay the onset of, and potentially overcome, CDK4/6i resistance in ER+/HER2- breast cancer. Our findings also suggest that LIPH and CD36 may have predictive value in patients receiving CDK4/6i-based therapy.

Results

A metabolic loss-of-function screen identifies LIPH as a modulator of CDK4/6i response

To identify metabolic dependencies associated with CDK4/6i response in ER+/HER2- breast cancer, we performed a loss-of-function screen in MCF7 cells using a curated lentiviral shRNA library. The library comprised approximately 14,000 shRNA vectors targeting 2,752 genes encoding known human metabolic enzymes and transporters, defined by cross-referencing metabolic pathway maps with the KEGG database, as previously described[23]. In addition, the library included a set of control genes known to influence CDK4/6i response based on publicly available data, such as *RB1*. Successfully infected cells were maintained in culture for 10 days. At this time point, surviving cells were collected and used as the baseline reference population (MCF7 Day 0, **Figure 1A**). Genomic DNA was extracted to retrieve shRNA barcode sequences, which were quantified by next-generation sequencing (NGS, **Figure 1A**). This baseline analysis allowed us to identify shRNAs depleted under untreated conditions, corresponding to essential metabolic genes required for basal cell fitness. In parallel, infected cells (MCF7 Day 0, **Figure 1A**) were either left untreated (control, **Figure 1A**) or exposed for an additional 10 days to 80 nM

palbociclib (palbo 80 nM, **Figure 1A**), corresponding to the IC20 concentration (**Figure S1A**), a low dose that allowed maximizing the effects of the screen in searching for non-essential metabolic genes whose targeting is synthetic lethal when palbociclib is administered. shRNA abundance in the palbociclib-treated population was then compared with the baseline reference population using the MAGeCK algorithm[24] to identify genes whose loss selectively impaired cell fitness under CDK4/6i. The robustness of the screen was confirmed by the emergence of *RB1*, whose loss is associated with CDK4/6i resistance[25], as the top hit of the "desensitizers" gene list (**Figures 1B-1D**). Among the candidate synthetic lethal genes identified, *LIPH,* a phospholipase involved in LPA production[17], scored as a potential modulator of palbociclib response (**Figures 1B-1D**). To validate this observation, LIPH was transiently silenced in the ER+/HER2- breast cancer MCF7 and T47D cells, and depletion was confirmed at mRNA (**Figure 1E**) and protein levels (**Figures 1F, 1G, and S1B**). Consistent with the role of LIPH in catalyzing the conversion of PA into LPA, LIPH silencing significantly reduced both intracellular and extracellular LPA levels (**Figure 1H**), providing functional evidence that LIPH mediates LPA production in these cells. Notably, LIPH silencing significantly impaired long-term cell survival (10 days) in both MCF7 and T47D cells treated with palbociclib (**Figure 1I**). This phenotype was also observed following ribociclib and abemaciclib treatment, indicating that LIPH depletion broadly sensitizes ER+ breast cancer cells to FDA-approved CDK4/6i (**Figure 1I**). Similar effects were observed following palbociclib treatment in additional ER+/HER2- breast cancer cell models, including HCC1428 and SUM44 cells, in which LIPH silencing (**Figures S1C, S1D**) significantly enhanced the effects of palbociclib (**Figure S1E**). Short-term treatment (3 days) with CDK4/6i also induced synthetic lethality in LIPH-silenced MCF7 and T47D cells (**Figure S1F**), suggesting that the sensitization occurs prior to long-term exposure. Moreover, CRISPR interference (CRISPRi)-mediated LIPH depletion (**Figure S1G, S1H**) phenocopied the effects observed following transient silencing and significantly enhanced palbociclib sensitivity in MCF7 cells (**Figure S1I**).

LPA signaling mediates the sensitization to CDK4/6i induced by LIPH depletion

Since LIPH silencing reduced both intracellular and extracellular LPA levels, we hypothesized that the sensitization to CDK4/6i is mediated by impaired LPA-dependent signaling. To test this, we supplemented LIPH-depleted cells with exogenous LPA, restoring cell survival in MCF7 and T47D cells treated with palbociclib (**Figure 2A**). Since LPA signaling has been associated with pathways involved in cell survival and stress adaptation[26], we explored potential downstream mediators activated upon LPA exposure. Notably, LPA administration induced the phosphorylation (i.e., activation) of AMPK and p38 in a time-dependent manner (**Figure 2B**). LPAR2 has been reported to be highly expressed in breast cancer[27]. Moreover, in two independent ER+/HER2− breast cancer cohorts, high *LPAR2* expression is associated with unfavorable clinical outcome, as reflected by reduced relapse-free survival (RFS, HR = 1.27, log-rank p = 0.0407) and OS (HR = 1.45, log-rank p = 0.0099, **Figure S2A**). This receptor also emerged as the most expressed LPAR family member in our cellular model by interrogating our publicly available transcriptomic data (**Figure S2B**). We therefore reasoned that LPAR2 could mediate the effects induced by LPA. Indeed, LPAR2 inhibition partially impaired the LPA-induced phosphorylation of AMPK and p38 (**Figure 2B**) and, accordingly, potentiated the reduction of cell survival induced by palbociclib

administration in MCF7 cells at both 10 and 3 days (**Figures 2C and S2C**). Consistent with this model, pharmacological inhibition of AMPK or p38 phenocopied the upstream targeting of the LIPH-LPA-LPAR2 axis and induced synthetic lethality in combination with palbociclib following both long- and short-term treatment in MCF7 and T47D cells. (**Figures 2D, 2E and S2D, S2E**). These findings support a model in which the LPA-induced LPAR2 signaling promotes CDK4/6i response through AMPK/p38 pathway activation.

CD36 mediates the effects of LPA signaling on CDK4/6i response

To identify downstream effectors linking the LPA-LPAR2-AMPK/p38 axis to CDK4/6i response, we focused on CD36, a fatty acid transporter and lipid-sensing receptor, which was not present in the shRNA library. CD36 is induced downstream of AMPK/p38 signaling[28]. In addition, CD36 has been linked to proliferative capacity in breast cancer[29] and, in non-cancer models, to G1/S progression through the cyclin D1–CDK4 axis[30]. Together, these observations suggested that CD36 could connect LPA-dependent lipid signaling with the cell-cycle machinery targeted by CDK4/6i. Notably, LIPH silencing significantly reduced CD36 mRNA and protein levels in ER+ breast cancer cells (**Figures 3A-C and S3A**). To investigate whether CD36 contributes to the effects induced by LIPH depletion, MCF7 and T47D cells were treated with the CD36 inhibitor sulfosuccinimidyl oleate (SSO) in combination with CDK4/6i. SSO is an established pharmacological tool applied in preclinical models to interrogate the therapeutic potential of CD36 targeting[31]. In both cell lines, pharmacological CD36 inhibition significantly enhanced the effects of palbociclib, ribociclib, and abemaciclib following long-term exposure (**Figure 3D**), providing proof-of-concept that CD36 targeting can potentiate CDK4/6i activity. Comparable effects were observed after short-term treatment in MCF7 and T47D cells (**Figure S3B**), as well as following palbociclib administration in combination with SSO in HCC1428 and SUM44 cells (**Figure S3C**). To further validate CD36 as the relevant target of SSO-mediated sensitization and minimize the possibility of compound-specific off-target effects, the receptor was transiently silenced in MCF7 and T47D cells (**Figures 3E-G**). Genetic CD36 depletion significantly enhanced the sensitivity to CDK4/6i in both cell lines (**Figure 3H**). Moreover, short-term exposure to CDK4/6i similarly induced synthetic lethality in CD36-silenced MCF7 and T47D cells (**Figure S3D**). Together, these orthogonal pharmacological and genetic approaches identify CD36 as a functional downstream effector of the LPA signaling axis that modulates CDK4/6i response in ER+ breast cancer cells.

CD36 regulates CCND1 expression and cell cycle progression

Since CD36 has been linked to proliferative control and G1/S progression through modulation of the cyclin D1 (encoded by *CCND1*)/CDK4 axis[30], we investigated whether modulation of the LPA-LPAR2-CD36 signaling axis could affect cyclin D1 expression. Importantly, CD36 silencing reduced cyclin D1 protein levels in both MCF7 and T47D cells (**Figure 4A**). Consistently, LIPH depletion reduced both CD36 and cyclin D1 expression (**Figure 4B**), while pharmacological inhibition of LPAR2, p38, or CD36 also decreased cyclin D1 protein levels in MCF7 cells (**Figure 4C**). Together, these findings suggest that the LPA-LPAR2-AMPK/p38 signaling axis sustains cyclin D1 expression, at least in part through CD36-

dependent signaling. Since cyclin D1 is a key regulator of the G1/S cell cycle transition through activation of CDK4/6 and phosphorylation of RB[32], we next investigated whether LIPH or CD36 depletion could affect cell cycle progression. Flow cytometry analysis revealed that both LIPH and CD36 silencing increased the percentage of cells in G0/G1 phases, with a concomitant reduction of cells in S and G2/M phases (**Figures 4D, 4E**), indicating impaired cell cycle progression. These observations were further confirmed using the fluorescent ubiquitination-based cell cycle indicator (FUCCI-3) reporter system, which allows real-time visualization of cell cycle progression in living cells[33,34]. In line with the FACS analysis, LIPH- and CD36-silenced cells showed increased Cdt1-mKO2 (orange) and SLBP-Turquoise2 (blue) fluorescence, indicative of an accumulation of cells in G1 and early cell-cycle phases, together with reduced Clover-Geminin fluorescence (green), consistent with a decrease in cells progressing through S/G2/M phases (**Figures 4F, 4G**). To further support the involvement of LPA signaling in this pathway, exogenous LPA administration restored CD36 and cyclin D1 expression in LIPH-silenced cells (**Figures 4H, 4I**). These findings support a model in which LIPH-derived LPA sustains the CD36-CCND1 signaling axis involved in CDK4/6i response in ER+ breast cancer cells.

CD36 targeting enhances endocrine therapy and CDK4/6i response in ER+ therapy-resistant breast cancer models

Given that CD36 inhibition potentiates CDK4/6i effects in endocrine-sensitive models, we next asked whether this signaling axis could also contribute to acquired resistance to CDK4/6i. Palbociclib-resistant (PalboR) MCF7 cells displayed increased LIPH, CD36, and cyclin D1 expression compared to parental cells (**Figures 5A-5C**), suggesting activation of this pathway upon acquisition of resistance. Functionally, PalboR cells exhibited enhanced sensitivity to the CD36 inhibitor SSO than parental cells (**Figure 5D**), supporting a potential increased reliance on CD36 signaling in the resistant setting. Since CDK4/6i are clinically administered in combination with endocrine therapy in ER+/HER2- breast cancer[1], we next evaluated whether CD36 targeting could further enhance the efficacy of these clinically relevant combinatorial treatments. In parental MCF7 and T47D cells, addition of SSO to palbociclib combined with either tamoxifen or fulvestrant further reduced cell survival compared to the corresponding double treatments (**Figures 5E, 5F**). We next extended these observations to endocrine therapy-resistant models, including tamoxifen-resistant (TamR) and fulvestrant-resistant (FulvR) MCF7 cells. Notably, combined treatment with palbociclib and SSO significantly impaired cell survival in the resistant derivatives (**Figure 5G, 5H**), indicating that CD36 targeting can enhance CDK4/6i efficacy also in ER+ endocrine-resistant breast cancer cell derivatives.

LIPH and CD36 expression are associated with poor clinical outcome in ER+ breast cancer

To assess the clinical and translational relevance of the LIPH-CD36 axis, we evaluated the effects of CD36 inhibition in PDOs. SSO significantly potentiated the effects of palbociclib in two independent ER+ breast cancer PDO models (**Figures 6A, 6B**). Similar effects were observed upon ribociclib treatment (**Figure 6C**), further supporting the therapeutic potential of CD36 targeting in combination with CDK4/6i. We next examined whether the LIPH–CD36 axis was associated with clinical response to CDK4/6i-based

therapy. Since median PFS in this setting is ~23 months[35], we used stringent cutoffs to enrich for patients with clearly divergent outcomes, defining poor responders as those with PFS < 9 months and long responders as those with PFS > 36 months. Notably, poor responders displayed higher LIPH and CD36 scores compared to long responders (**Figures 6D, 6E**). Finally, to further assess the prognostic relevance of the described pathway, we retrospectively analyzed an independent cohort of patients with ER+/HER2- breast cancer stratified according to high versus low LIPH or CD36 mRNA expression. In line with our preclinical findings, elevated *LIPH* or *CD36* expression significantly correlated with reduced RFS (LIPH, HR = 1.21, log-rank p = 0.0513; CD36, HR = 1.41, log-rank p = 0.0286) in breast cancer patients (**Figure 6F, 6G**). Finally, ER+/HER2− breast cancer patients were stratified according to the combined expression of LIPH, LPAR2, and CD36, as this would reflect the concomitant presence, and possibly activation, of the molecular players described in our model. Patients with high expression of the combined LIPH/LPAR2/CD36 mean-expression signature displayed significantly shorter post-progression survival (PPS, HR = 2.03, log-rank p = 0.0079, **Figure 6H**), suggesting that activation of this signaling axis may influence disease behavior beyond initial relapse. Together, these findings support the clinical relevance of the LIPH-CD36 signaling axis in ER+/HER2- breast cancer progression and CDK4/6i response and suggest its potential utility both as therapeutic vulnerability and as candidate biomarker of disease outcome.

Discussion

The introduction of CDK4/6i changed the therapeutic approach in ER+/HER2− breast cancer, but resistance remains a clinical challenge, particularly in the advanced stages. While most described resistance mechanisms converge on traditional cell-cycle reactivation via changes in RB, cyclin E, AURKA, PI3K/AKT/mTOR, or KRAS signaling[3,36], emerging evidence points toward a crucial role for metabolic rewiring[5–7]. Our group and others have previously demonstrated that lipid metabolic reprogramming supports ER+ breast cancer progression and influences therapy response and resistance[37–39]. In this study, we uncover the LIPH–LPA–LPAR2–CD36 axis as a previously unrecognized lipid-driven signaling pathway that can regulate the response to CDK4/6i in ER+/HER2− breast cancer. Using an unbiased metabolic loss-of-function screen together with orthogonal genetic, pharmacological, and clinical validation, we demonstrate that targeting this pathway enhances sensitivity to multiple clinically approved CDK4/6i, and key players of this axis correlate with poorer therapy response and patient outcomes.

Importantly, the adopted screen revealed LIPH as a distinct metabolic vulnerability during palbociclib treatment. LIPH is a phospholipase A1 responsible for the generation of LPA, a bioactive lipid mediator known to promote proliferation, survival, migration, and therapy adaptation across multiple cancer types[17]. Transient silencing and CRISPRi-mediated LIPH depletion in ER+ breast cancer models confirmed the sensitization not exclusively to palbociclib, but also to ribociclib and abemaciclib, indicating that this vulnerability spans across the whole CDK4/6i class. Furthermore, LIPH depletion decreased LPA levels directly connecting this genetic hit to its reported biochemical function: driving

LPA production. Our functional data indicate that LIPH-dependent LPA production functions as an upstream signal that sustains cell viability during CDK4/6i exposure. Indeed, exogenous administration of LPA rescued LIPH-depleted cells from CDK4/6i-induced cell cycle arrest and subsequent toxicity, confirming that the absence of LPA is an essential player in driving the described CDK4/6i sensitization. On a mechanistic level, LPA administration triggered AMPK and p38 activation, and blocking LPAR2 diminished this effect and enhanced CDK4/6i efficacy, suggesting that LIPH-derived LPA can signal through LPAR2 to activate AMPK/p38 and synergize with the cyclin D1-CDK4/6 axis in driving cell cycle progression. However, from a translational perspective, targeting this cascade at the level of LIPH or its cognate receptors presents major challenges. Crucially, to our knowledge, there are currently no clinically approved compounds or targeted therapies that directly inhibit LIPH[40]. Moreover, attempting to block the cascade at the receptor level is similarly problematic due to the highly pleiotropic nature of LPARs, the main mediators of LPA signaling. Despite LPAR2 is the major isoform expressed in the ER+ breast cancer models used in our study, when translated into a more clinically relevant context (i.e., longer therapy administration), multiple parallel LPARs could easily bypass a specific receptor blockade to sustain downstream signaling. Indeed, other LPARs have been documented in diverse breast cancer subtypes and could potentially be involved in an LPA-induced LPARs molecular rewiring[20,41]. Because of these limitations, we made the strategic decision to target the pathway downstream of the LPARs at the level of CD36, which emerged from our investigation as a more viable and robust node for therapeutic intervention, although it was not identified in our primary screen because the gene was not present in the custom shRNA library reference we used[23]. CD36, a membrane glycoprotein, acts as both a scavenger receptor and a long-chain fatty acid transporter, allowing cells to maintain metabolic and redox homeostasis[42], and, in cancer cells, it has been associated with cancer progression, metastasis, stemness, and therapy resistance[43,44]. Notably, CD36 has been previously associated with AMPK/p38 signaling and with the regulation of proliferative programs[28,29], including cyclin D1–CDK4-mediated G1/S cell-cycle progression, making it a plausible molecular link between lipid signaling and cell-cycle control. Conceptually, this study advances our understanding by positioning CD36 as the downstream effector of the lipid-signaling cascade initiated by LPA and culminating in cyclin D1 regulation, thus bridging lipid signaling to the core cell-cycle machinery. LIPH depletion actively lowered CD36 expression, while both pharmacological inhibition and genetic silencing of CD36 improved CDK4/6i efficacy. Utilizing these distinct, orthogonal approaches reduces the chance that the results obtained using the CD36 targeting compound SSO could stem from compound-specific off-target effects, reinforcing the role of CD36 as a key mediator. Interestingly, the association between LPA signaling and CD36 may reflect a feature of cells exposed to CDK4/6i that might operate independently of the canonical capacity of CD36 in lipid transport and metabolic fueling. Instead, CD36 may act as a signaling hub or scaffold required to sustain the LPA-LPAR2 mediated pro-survival programs in line with previously published studies on the role of LPA signaling in proliferation and resistance and CD36 in oxidative stress adaptation and altered cellular signaling

Since a prolonged CDK4/6i exposure is known to induce a durable growth-arrest state often associated with senescence, LPA-induced LPAR2 signaling may contribute to the adaptive stress-response

mechanisms that allow cells to withstand this therapeutic pressure[45]. While we did not look directly at senescence, LPA-induced LPAR2 signaling is known to regulate stress responses and growth arrest[46], suggesting this pathway might broadly support cell survival under CDK4/6i therapy pressure. Under CDK4/6i, this adaptive response ultimately converges on CD36 and cyclin D1, linking lipid-mediated signaling directly to cell-cycle control. Our findings support this link, showing that the LIPH–LPA–LPAR2–CD36 axis sustains cyclin D1 expression, thus allowing the cell cycle to move forward. Knocking down CD36 lowered cyclin D1 levels in ER+ breast cancer cells, while LIPH depletion decreased both CD36 and cyclin D1. Pharmacological targeting of LPAR2, p38, or CD36 mirrored these results, and supplying exogenous LPA increased (i.e., reverted) CD36 and cyclin D1 expression in LIPH-silenced cells. Together, these data suggest a model where LIPH-derived LPA sustains CD36–cyclin D1 activation via LPAR2–AMPK/p38 signaling. Something that was not expected and reinforced the relevance of the described molecular mechanism and potential translational relevance is that this pathway remains active in therapy-resistant contexts. Indeed, cells resistant to palbociclib expressed higher levels of LIPH, CD36, and cyclin D1 than their parental counterparts, suggesting the axis sustains and drives CDK4/6i adaptation. Such resistant models were also more sensitive to CD36 inhibition than parental cells, indicating an acquired dependency on CD36-associated signaling during therapy resistance acquisition. Because CDK4/6i are combined with endocrine therapies in the clinic management of advanced and high-risk breast cancer patients, the fact that CD36 inhibition improved palbociclib efficacy when combined with endocrine agents (e.g., tamoxifen or fulvestrant) in the sensitive setting is highly relevant. Moreover, combining palbociclib with SSO compromised the survival of cells resistant to tamoxifen or fulvestrant, suggesting that targeting CD36 could enhance CDK4/6i activity across multiple distinct clinical resistance profiles. Patient-derived models and analysis of clinical datasets reinforce the clinical value of these findings. In PDOs, CD36 inhibition potentiated the effects of both palbociclib and ribociclib in two independent ER+ breast cancer models. Looking at clinical data, ER+/HER2- breast cancer patients who responded poorly to CDK4/6i-based regimens exhibited higher baseline LIPH and CD36 scores than long-term responders. Furthermore, retrospective analysis of an independent ER+/HER2– cohort showed that high expression of LIPH, LPAR2, or CD36 correlated with poorer survival, pointing to the potential predictive and prognostic value of the described signaling-molecular axis. Collectively, our findings identify a LIPH-generated LPA signaling network that drives response to CDK4/6i by regulating CD36 and cyclin D1 via the LPAR2–AMPK/p38 pathway. Moreover, targeting CD36, or disrupting the wider LIPH–LPA–LPAR2–CD36 axis, offers a potential strategy to enhance the efficacy of CDK4/6i and retard or reverse therapy resistance.

Limitations of the study

A few limitations of the study warrant to be highlighted. First, while SSO is a valuable, well-established preclinical tool for targeting CD36, it is not a clinically approved drug. Therefore, to assess the true translational impact and clinical feasibility of CD36 targeting will require optimizing and testing advanced pharmacological strategies, such as small-molecule inhibitors or therapeutic antibodies. Second, although our data indicate a clear LIPH/LPA-activated cascade via LPAR2 to AMPK/p38 and

CD36/cyclin D1, we cannot entirely exclude the influence of other LPARs or alternative lipid species. Third, the exact molecular mechanism by which CD36 dictates cyclin D1 expression remains incomplete: it may occur via non-canonical signaling mechanisms, altered fatty acid uptake, lipid signaling intermediates, downstream transcriptomic shifts, or changes in protein stability. Furthermore, CCND1 amplification occurs in ~10–20% of ER+/HER2- breast tumors and represents a genomic context in which upstream transcriptional regulation of cyclin D1 via the LIPH–CD36 axis might be functionally subordinate. Whether the therapeutic benefit of CD36 targeting is preserved in CCND1-amplified tumors, potentially through CCND1-independent mechanisms such as lipid metabolic support or stress adaptation under CDK4/6i, remains an open question that future studies should address. Finally, while our retrospective clinical data connect this pathway to survival and poor drug response, prospective validation in larger patient cohorts is needed before any component of this axis can be adopted as a clinical biomarker.

Materials and Methods

Study design

This study combines pooled functional genetic screening, preclinical cellular models, PDOs, clinical cohorts of patients, and retrospective clinical analyses to investigate the role of the LIPH-LPA-AMPK/p38-CD36 signaling axis in modulating response to CDK4/6i in ER+/HER2− breast cancer. Functional validation was performed using transient gene silencing, CRISPRi, pharmacological inhibition, cell viability assays, cell cycle analyses, and molecular characterization in both sensitive and therapy-resistant breast cancer models. The number of biological replicates and all statistical analyses are indicated in the corresponding figure legends or Materials and Methods. Researchers were not blinded during experimental procedures, except for the evaluation of the immunohistochemistry (IHC) scoring.

Cell cultures and reagents

Human female breast cancer cells (MCF7 - HTB-22, RRID: CVCL_0031; T47D - HTB-133, RRID: CVCL_0553; HCC1428 - CRL-2327, RRID: CVCL_1252; SUM44, RRID: CVCL_3424) were obtained from ATCC and maintained at 37°C/5%CO_2 in phenol red-free RPMI 1640 medium (Gibco, #32404014) supplemented with 10% fetal bovine serum (FBS, Euroclone, #ECS0180L), 2 mmol/L glutaMAX (Gibco, #35050-061), 1% penicillin/streptomycin (Gibco, #15140122), and 1 nmol/L 17β-estradiol (E2, Sigma-Aldrich, #E2758). In addition to the parental cell lines, we used drug-resistant MCF7 derivatives, including tamoxifen-resistant (MCF7-TamR), fulvestrant-resistant (MCF7-FulvR), and palbociclib-resistant (MCF7-PalboR) cells. Resistant cell lines were established through continuous exposure to progressively increasing concentrations of tamoxifen, fulvestrant, or palbociclib until reaching final concentrations of 1 µmol/L, 100 nmol/L, and 1 µmol/L, respectively. Drug selection was maintained for a minimum of 20 weeks, allowing for the selection and stabilization of cells with resistant phenotypes, distinct from the parental counterparts[12,47]. Resistant cells were continuously cultured in the same phenol red-free RPMI 1640 medium described above, with the corresponding selecting drug maintained in the culture medium.

These models were used to evaluate translationally relevant mechanisms of resistance, as they recapitulate clinically relevant therapeutic settings. HEK293T cells (CRL-3216, RRID: CVCL_0063), used for lentiviral particle production, were cultured in DMEM high glucose (Euroclone, #ECB7501L) supplemented with 10% FBS and 1% penicillin/streptomycin. All cell lines were short tandem repeat tested, amplified, stocked, routinely subjected to mycoplasma testing, and once thawed, were kept in culture for a maximum of 10 passages to minimize passage-related phenotypic drift. Palbociclib (PD0332991, #HY-50767), ribociclib (LEE011, #HY-15777), and abemaciclib (LY2835219, #HY-16297A) were purchased from MedChemExpress, dissolved in DMSO, and used at the indicated concentrations as described in Figure Legends. Tamoxifen (#T2859) and fulvestrant (ICI182,780, #I4409) were purchased from Santa Cruz Biotechnology, dissolved in ethanol and DMSO, respectively, and used at the appropriate concentration as described in Figure Legends. The LPAR2 inhibitor (LPAR2i, H2L5186303, #HY-107616), the AMPK inhibitor (AMPKi, BAY-3827, #HY-112083), the p38 inhibitor (p38i, adezmapimod, #HY-10256), and the CD36 inhibitor (sulfosuccinimidyl oleate sodium, SSO, #HY-112847A) were purchased from MedChemExpress, dissolved in DMSO, and used at the indicated concentrations as described in Figure Legends.

Pooled shRNA functional screening

MCF7 cells were transduced with a custom shRNA library targeting genes involved in cellular metabolism[23] at a multiplicity of infection (MOI) of 0.4. The following day, puromycin-containing medium was added to select for transduced cells. After 3 days of selection, cells were switched to puromycin-free medium and maintained in culture for an additional 10 days. Subsequently, cells were pooled and split into two technical replicates for each of two experimental conditions. To maintain a 400× library representation throughout the screen, infected MCF7 cells from each replicate were seeded at low density (1×10^6 cells per T175 flask) and propagated until the experimental endpoint. Cell populations were either left untreated (control group) or treated with 80 nM palbociclib, with the drug replenished every 3 days. At the endpoint of the screen, cells were harvested and submitted to the Sigma-Aldrich MISSION® Op. Deconvolution Service for genomic DNA isolation and subsequent sequencing analysis. Quality control was then performed using R software (https://www.R-project.org/). Statistical analysis of the screen (day 0 vs palbociclib-treated population) was carried out using the MAGeCK Robust Rank Aggregation (RRA) module[24] and the R package MAGeCKFlute[48]. Minimum effect size was delimited using Log Fold Change (LFC) of each Day 0 comparison, as well as the difference between them to exclude genes with correlated essentiality. For this, cutoffs were established at the distribution mean ± 1.5*SD. To identify palbociclib synthetic lethality and viability hits, we focused on those genes that were between those cutoffs (*i.e.*, not altered) in the untreated control cells, but below the lower cutoff in the palbociclib-treated cells. This allowed us to exclude essential genes and identify differential depletion or enrichment of shRNAs occurring only in the treated cells, which points towards synthetic lethality and viability, respectively.

Cell viability assay for PDO models

PDOs were generated:

(1) the BB7217T2 PDO from an ascitic metastatic sample, processed as previously described[49]. The patient previously received adjuvant chemotherapy consisting of epirubicin and cyclophosphamide followed by a taxane (EC-T), as well as sequential endocrine therapy with tamoxifen, letrozole, and anastrozole. After developing metastatic disease, first-line treatment consisted of fulvestrant plus ribociclib for 7 months, followed by second-line capecitabine. Third-line therapy was everolimus combined with exemestane for 6 months. At the time of sample collection, the patient was receiving vinorelbine as fourth-line treatment. In brief, 5,000 cells isolated from the ascitic effusion were resuspended in 40 µL of a cold Matrigel-media mixture (1:1) and seeded as a dome in 24-well plates. Matrigel domes were allowed to solidify for 30 minutes at 37°C before the addition of organoid culture media, composed of advanced DMEM/F12 (Thermo Fisher, #12634010) supplemented with 5% FBS, 2 mM L-glutamine, 10 mM 4-(2-hydroxyethyl)-1-piperazineethanesulfonic acid (HEPES, Thermo Fisher, #11330032), 100 U/mL penicillin + 0.1 mg/mL streptomycin, 1 µg/mL hydrocortisone (Sigma Aldrich, #H0888), 10 ng/mL epidermal growth factor (EGF, Miltenyi Biotec, #130-097-751), 1 mM N-acetyl cysteine (NAC, Sigma Aldrich, #A9165), 100 ng/mL fibroblast growth factor 2 (FGF2, Miltenyi Biotec, #130-093-837), and 10 µM of the rho-associated protein kinase (ROCK) inhibitor Y-27632 (APExBIO, #B1293). After 7 days of growth, established organoids were treated with 50 µM SSO in combination with 1 µM palbociclib or 75 µM SSO in combination with 500 nM ribociclib. Plates were then placed inside the Incucyte S5 live-cell imaging system, and images were taken every 24 hours at 4x magnification. The medium was replenished every 3 to 4 days. At the end of each experiment, images were analyzed using Incucyte® Organoid Analysis Software. Organoid masks were generated based on organoid size and morphology, and the average organoid area was quantified over time to assess treatment-induced changes in growth.

(2) The organoid model HBCx-139-org was derived from the PDX HBCx-139, established from a bone metastasis of a ER+ breast cancer patient[50]. The HBCx-139-org was established as detailed in Soosainathan et al.[51]. Briefly, PDX tumors were dissociated with an enzymatic solution, embedded in 100 µL Matrigel (Corning, 354230), and plated in six-well tissue culture plates onto a 70 µL Matrigel base layer. After a 30-minute incubation, organoid medium consisting of advanced DMEM/F12 with 5% FBS, 10 mmol/L HEPES, 1X Glutamax, 1 mg/mL hydrocortisone, 50 mg/mL gentamicin, 10 ng/mL hEGF, 100 ng/mL FGF2, 10 mmol/L Y-27632, and 1 mmol/L N-acetyl cysteine was added. Medium was replenished every 3 to 4 days. Organoids were dissociated using TrypleExpress (Life Technologies, 12605010) for 20 minutes. Established organoids were treated with palbociclib and SSO for 72 hours in quadruplicate combined at different concentrations and cell viability assessed using CellTiter-Glo® 3D Cell Viability Assay (Promega, G9682, v/v) following 20-minute incubation at room temperature.

Viability assay

Human ER+/HER2- breast cancer cells were seeded into 12-well plates at $3–5×10^4$ cells per well in either standard conditions (see “Cell cultures and reagents” sub-section) or experimental conditions such as

drug administration, as described in Figures and Figure Legends. Cell counts were performed at least in triplicate by two analysts under a 10x objective according to the standard methodology. Alternatively, plates were stained with crystal violet (triphenylmethane dye 4-[(4-dimethylaminophenyl)-phenyl-methyl]-N, N-dimethyl-alanine, Sigma-Aldrich, #C6158), dried overnight, and the crystal violet within the adherent cells was solubilized using 500 µL/well of 2% SDS. The absorbance was evaluated at 595 nm using a VICTOR Nivo microplate reader.

Transient siRNA transfection

Human ER+/HER2- breast cancer cells were seeded into 6-well plates (4×10^5 per well) to achieve 70% confluence the following day, when cells were transfected with 50 nmol/L siGENOME human siRNA targeting LIPH (siLIPH, GE Healthcare Dharmacon, #M-008689-01), or 50 nmol/L siGENOME human siRNA targeting CD36 (siCD36, GE Healthcare Dharmacon, #M-010206-01), and the respective negative control (non-targeting small interfering RNA, siCTR, GE Healthcare Dharmacon, #D-001210-01) using Lipofectamine RNAiMAX Reagent (Thermo Fisher Scientific, #13778-150) and Opti-MEM (Gibco, #31985062) accordingly to manufacturer's instructions. The functional analyses were performed 48 hours, 72 hours, or 10 days after transfection as described in Figure Legends.

Lentiviral particles production and cell transduction

Lentiviral particles were generated using HEK293T cells cultured in 6 cm culture plates (5×10^5 cells per plate) and transfected via a polyethyleneimine (PEI)-mediated protocol (MedChemExpress, #HY-K2014) with a mixture of three transfection plasmids used as follows: 8.4 µg of pLL3.7m-mTurquoise2-SLBP(18-126)-Geneticin or pLL3.7m-Clover-Geminin(1-110)-IRES-mKO2-Cdt(30-120)-Hygromycin, kindly provided by Dr Sdelci[34]; 1.1 µg of pCMVR8.74 (AddGene #22036, RRID: Addgene_22036) and 0.45 µg of pMD2.G (AddGene #12259, RRID: Addgene_12259). 6 hours later, the medium was replaced with fresh growth medium. After 48 hours, the media supernatants were collected, centrifuged at 550 × g for 5 minutes, and filtered through a 0.45 µm filter. The supernatant containing the virus was stored at 4 °C for the subsequent cell infection.

Lentiviral CRISPRi-mediated knockdown

MCF7 cells were seeded into 6-well plates (4×10^5 per well) to achieve 50-70% confluence the following day, when cells were transduced using CRISPRi human LIPH all-in-one sgRNA lentiviral system (Horizon, #FE6VSGH12437). Briefly, lentiviral particles were gently diluted into serum-free basal cell culture medium to achieve a MOI of 1. The growth medium was aspirated from the wells and replaced with 0.5 mL of the transduction mixture containing lentiviral particles. Cells were incubated with the lentiviral mixture for 4–6 hours. Following this incubation, the transduction medium was supplemented with 1.5 mL of serum-containing cell culture medium, and incubation was resumed. 72 hours after the transduction, MCF7 cells were resuspended in the sorting buffer solution composed of dulbecco's phosphate buffered saline (PBS, Euroclone, #ECB4053) with 1% bovine serum albumin (BSA, Sigma-Aldrich, #A1900), MgCl2 (2.5 mM, Sigma-Aldrich, #M9272), EDTA (5 mM, Sigma-Aldrich, #E9884), HEPES

(25 mM), and DNase I (5U/mL, Thermo Fischer Scientific, #EN0521), and subsequently subjected to FACS sorting using FACSMelody cell sorter (BD Biosciences) to isolate and enrich the enhanced green fluorescent protein positive ($EGFP^+$) transduced cells. The MCF7 CRISPRi cells were then analyzed for the knockdown of the gene of interest by qRT-PCR and immunofluorescence analysis.

Western blotting

Human ER+/HER2- breast cancer cells were washed with PBS and lysed on ice using 1x Laemmli Sample Buffer (Bio-Rad, #161-0737) supplemented with protease (Sigma-Aldrich, #P8340) and phosphatase inhibitors (Sigma-Aldrich, #P0044). Protein concentrations were measured using the BCA assay (Sigma-Aldrich, #1003290033). 40–50 µg of cell lysate were loaded into precast sodium dodecyl sulfate-polyacrylamide gel electrophoresis (SDS-PAGE) gels (Bio-Rad, #456-8096) and then transferred onto a nitrocellulose membrane by Trans-Blot Turbo Transfer Pack (Bio-Rad, #170-4157). The immunoblots were incubated in PBS-T (PBS with 0.05% Tween-20) containing 5% non-fat dry milk at room temperature for 1 hour and then probed with primary and appropriate secondary antibodies. The following antibodies were used: LIPH, (Novus Biologicals, #NBP3-46019; Proteintech, #66303-1-Ig), LPAR2 (Thermo Fischer Scientific, #PA5-102074), AMPK (Cell Signaling, #2532), pAMPK (phospho-AMPK alpha (Thr172), Cell Signaling, #2535), p38 MAPK (Cell Signaling, #9212), p-p38 (phospho-p38 MAPK (Thr180/Tyr182), Cell Signaling, #9211), CD36 (Proteintech, #66395-1-Ig; Thermo Fisher Scientific, #PA5-12514), cyclin D1 (Cell Signaling, #2922), HSP90 (Santa Cruz Biotechnology, #sc-69703), all diluted 1:1.000 in PBS-T containing 5% non-fat dry milk. Blots were processed in parallel when it was not possible to run on the same gel.

RNA extraction and quantitative Real-Time PCR (qRT-PCR) analysis

Total RNA was extracted using the RNeasy plus kit (QIAGEN, #74134), quantified using Nanodrop 1000 (Thermo Fisher Scientific), and 500 ng were reverse transcribed using the iScript gDNA Clear cDNA Synthesis Kit (Bio-Rad, #172-5035). qRT-PCR analysis was performed using the CFX96 Touch Real-Time PCR Detection System (Bio-Rad) using TaqMan Universal PCR Master Mix (Thermo Fisher Scientific, #4305719). The following probes were used: LIPH, CD36, CCND1 (ID: Hs00975890_m1, ID: Hs00354519_m1, ID: Hs00765553_m1, Thermo Fisher Scientific, #4453320). Data were normalized on TATA-Box Binding Protein (TBP, ID: Hs00427620_m1, Thermo Fischer Scientific, #4453320) or RNU48 (ID: Hs04931161_g1, Thermo Fisher Scientific, #4453320). The relative quantity was determined using $^{\Delta\Delta}$Ct by the CFX Maestro software (Bio-Rad).

Droplet digital PCR (ddPCR)

ddPCR was performed using the QX200 ddPCR system (Bio-Rad). Reactions were prepared in a final volume of 20 µL containing 5 µL of ddPCR Multiplex Supermix, the appropriate primer sets, DNase/RNase-free sterile water, and 10 ng of cDNA. Each reaction mixture was combined with 70 µL of droplet generation oil for probes and loaded into a DG8 droplet generator cartridge. Droplets were generated using the QX200 droplet generator and subsequently transferred to a 96-well PCR plate. PCR

amplification was carried out in a thermal cycler equipped with a deep-well reaction module under the following conditions: 95°C for 5 minutes, followed by 40 cycles of 94°C for 30 seconds and 58°C for 1 minute, then 98°C for 10 minutes, 4°C for 30 minutes, and a final hold at 4°C. Following amplification, droplets were analyzed using the QX200 droplet reader, which measures the fluorescence intensity of individual droplets. Droplets were classified as positive or negative according to the presence or absence of the target sequence. Absolute CD36 and CCND1 transcript concentration (copies/µL) was determined using QuantaSoft software (version 2.1, Bio-Rad), and data were normalized to TBP expression.

LPA level measurement

MCF7 cells were seeded into 6-well plates ($4x10^5$ cells per well) in either standard conditions or experimental conditions, as described in Figure Legends. LPA levels were measured with the Human lysophosphatidic acid ELISA Kit (MyBioSource, #MBS1609797), according to the manufacturer's instructions. Briefly, endogenous LPA competes with a biotinylated antigen for binding to a capture antibody; absorbance is measured at 450 nm, and LPA levels are calculated from a standard curve.

Flow cytometry analysis

5-ethynyl-2´-deoxyuridine (EdU) incorporation

To analyze DNA replication in proliferating cells, the Click-iT™ EdU Alexa Fluor™ 488 kit (Thermo Fisher Scientific, #C10425) was utilized according to the manufacturer's instructions. Briefly, breast cancer cells ($3–5×10^4$ cells per well) were seeded into 12-well plates and subjected to the experimental procedure described in Figure Legends. The day after, cells were treated with 10 µM EdU for 2 hours at 37°C, washed with 1% BSA-containing PBS, and subsequently labeled with Alexa Fluor 488 fluorescent azide according to the Click-iT™ reaction protocol. Live cells were finally analyzed by flow cytometry using a FACSCanto II (BD Biosciences) to determine EdU incorporation. A total of $1×10^4$ events were acquired per sample, and the percentage of EdU-positive cells was used as a measure of DNA synthesis/cellular proliferation and was calculated using the FlowJo software.

Cell cycle progression

For the analysis of the cell cycle, breast cancer cells ($3–5×10^4$ cells per well) were seeded into 12-well plates and subjected to the experimental procedure described in Figure Legends. Then, cells were washed with PBS, fixed with 70% cold ethanol (-20°C), and incubated for 4 hours on ice. After washing with PBS, cells were stained for 20 minutes at room temperature in PBS with 50 ug/mL propidium iodide (PI, Thermo Fisher Scientific, #P1304MP) and 10 mg/mL RNase (Thermo Fisher Scientific, #R1253), and subsequently analyzed by flow cytometry using a FACSCanto II (BD Biosciences). The percentage of breast cancer cells in each phase of the cell cycle (G0/G1, S, G2/M) was calculated using the FlowJo software.

Immunofluorescence

Breast cancer cells were seeded onto glass coverslips ($3x10^4$ per well of a 12-well plate) to have a 40-50% confluence and subjected to the experimental procedure described in Figure Legends. The day after, cells were fixed in 4% formaldehyde for 10 minutes and permeabilized with 0.2% Triton X-100 (Sigma-Aldrich, #T8787) in PBS for 10 minutes, followed by blocking for 1 hour with 5% FBS in PBS. Subsequently, cells were incubated overnight at 4°C with primary antibodies anti-LIPH (Proteintech, #66303-1-Ig) or anti-CD36 (Proteintech, #66395-1-Ig) diluted 1:250 in 1% BSA-containing PBS. The day after, cells were washed three times with PBS and incubated with a 1:1000 dilution of anti-Rabbit IgG Alexa Fluor 488 (Thermo Fisher Scientific, #A11034) in 1% BSA-containing PBS for 1.5 hours at room temperature in the dark. For nuclei staining, fixed cells were incubated with Hoechst 33342 (Thermo Fisher Scientific, #H3570) for 10 minutes at room temperature. Sample images were acquired using a TCS SP8 microscope (Leica Microsystems) with LAS-AF image acquisition software. The quantification of LIPH and CD36 fluorescence intensity was performed using LAS-X software.

FUCCI-3 Reporter MCF7 cell line generation

To establish a stable FUCCI-3 system, MCF7 cells were seeded into 6-well plates ($4×10^5$ per well) and infected the next day with lentivirus for 72 hours together with 10 µg/mL polybrene (Santa Cruz Biotechnology, #sc-134220). Following transduction, cells were cultured in complete medium containing 200 µg/mL Geneticin (Thermo Scientific, #10131027) and 150 µg/mL Hygromycin (Sigma-Aldrich, #H3274) to select for successfully transduced cells, with the selection process lasting four to seven days. To maintain stable FUCCI-3 reporter expression and preserve population homogeneity, FUCCI-3-expressing cells were cultured for no longer than one month. To determine the cell cycle phases in the MCF7 FUCCI-3 cell line using confocal microscopy, the excitation filter 390–420 nm and emission 430–500 nm were used to measure SLBP-Turquoise2 signal, the excitation filter 460–490 nm and emission 500–550 nm were used to measure Clover-Geminin signal, and the excitation filter 530–560 nm and emission 570–650 nm were used to measure Cdt1-mKO2 signal. Specifically, the G0/G1 cell population is characterized by high Cdt1-mKO2 (orange) expression together with low Clover-Geminin (green) and increased SLBP-Turquoise2 (blue) levels. Cells in the G1/S transition display enhanced Clover-Geminin expression, whereas cells progressing through G2/M exhibit the highest levels of Clover-Geminin, accompanied by a progressive loss of SLBP-Turquoise2 and Cdt1-mKO2 expression. The percentage of breast cancer cells in each phase of the cell cycle was calculated using Fiji software.

Immunohistochemistry (IHC)

Formalin-fixed paraffin-embedded blocks of tumor tissues were from cases of metastatic patients with ER+/HER2- breast cancer from *Azienda Ospedaliero Universitaria Careggi* (AOUC), Hospital of Florence. Breast cancer specimens were fixed in 4% paraformaldehyde and embedded in paraffin for histology and IHC analysis. Sections were stained with the antibodies specific for LIPH (Proteintech, #66303-1-Ig) and CD36 (Proteintech, #66395-1-Ig). The specificity of the antibodies was established using healthy human pancreas sections for LIPH and healthy human liver sections for CD36 as positive controls. IHC was performed using the Leica BOND-MAX automated system (Leica Microsystems). Slides were developed

with 3'3-diaminobenzidine (Bond Polymer Refine Detection, Leica Microsystems) and counterstained with hematoxylin. Images were acquired using a slide scanner (Aperio LV1; Leica Biosystems), and the LIPH/CD36 staining intensity of tumor cells was scored by a breast pathologist (SB) as strong (3+), moderate (2+), or weak (1+). Informed consent was obtained from all patients and the study was conducted in accordance with the Declaration of Helsinki and Good Clinical Practice guidelines as well as authorized by the local Ethics Committee.

In silico analysis of human datasets

LIPH, *LPAR2*, and *CD36* mean expression signature survival analysis was performed using Km-plotter (http://kmplot.com/analysis/) by evaluating PPS in ER+/HER2- breast cancer patients and applying the best-performing cut-off to maximize prognostic resolution. *LPAR2* OS analysis was also performed using Km-plotter in the same molecular subtype. The curated dataset of ER+/HER2- (assessed by array data) breast cancers included the gene expression and survival data of primary tumor patient specimens, selected independently of any adjuvant or local therapeutic intervention, belonging to the following datasets: GSE1456, GSE16446, GSE16716, GSE20271, GSE20685, GSE20711, GSE22093, GSE3494, GSE37946, GSE42568, GSE45255, GSE48390, GSE58812, GSE65194, GSE69031, GSE7390. The probes selected for each gene were: 235871_at (LIPH), 206723_s_at (LPAR2), 206488_s_at (CD36). *LIPH* and *CD36* survival analysis were performed in the ER+/HER2- METABRIC cohort[52] applying the optimal cut-off to stratify patients into high and low expression groups. The optimal cut-off was identified using the *surv_cutpoint* function from the R package *survminer* (https://rpkgs.datanovia.com/survminer/index.html).

Statistics and reproducibility

Statistics were performed using Prism 10 (GraphPad Software). Unless stated otherwise, all numerical data are expressed as the mean ± standard error of the mean (SEM). All experiments were conducted at least 3 times independently, with one or more technical replicates for each experimental condition tested. Unless stated otherwise, comparisons between 2 groups were made using the two-tailed, unpaired Student's t-test. Comparisons between multiple groups were made using one-way or two-way analysis of variance (ANOVA). Dunnett, Tukey, or Šidák post-testing analyses with a confidence interval of 95% were used for individual comparisons as reported in Figure Legends. Survival curves were estimated using the Kaplan-Meier method and compared using the log-rank test, while hazard ratios (HR) and 95% confidence intervals were calculated using Cox proportional hazards regression. Statistical significance was defined when $p < 0.05$. P-values are reported only when biologically relevant, as indicated in Figure Legends. When differences were not statistically significant or the comparison was not biologically relevant, no indication was reported in the figures.

Declarations

Resource availability

Lead contact

Further information and requests for resources and reagents should be directed to the lead contact, Andrea Morandi (andrea.morandi@unifi.it).

Materials availability

All unique/stable reagents generated in this study are available from the lead contact without restriction.

Data and code availability

All data reported in this paper will be shared by the lead contact upon request.

This paper does not report original code.

Any additional information required to reanalyze the data reported in this paper is available from the lead contact upon request.

Acknowledgements

The work was funded by Associazione Italiana Ricerca sul Cancro (AIRC) and Fondazione Cassa di Risparmio di Firenze (grant IG22941 and IG30325 to A.M.), PNRR M4C2-Investimento 1.4-CN00000041 CN3 “Sviluppo di Terapia Genica e Farmaci con Tecnologia ad RNA” funded by NextGenerationEU (to A.M.), PNRR “THE - Tuscany Health Ecosystem” ambito di intervento “1. Health” ECS00000017 funded by NextGenerationEU (to A.M), Swiss National Science Foundation (3200-0-242892 to S.R.).

Declaration of interests

I.M. declares consultant honoraria for Eli Lilly, Novartis, Gilead, AstraZeneca, Daiichi Sankyo, Menarini StemLine, MSD, and Pfizer. All the other authors declare no competing interests.

Declaration of generative AI and AI-assisted technologies in the writing process.

The illustration was created with BioRender.com. During the preparation of this manuscript, the authors used AI-assisted language tools to enhance clarity and readability. The authors critically reviewed and revised the manuscript and take full responsibility for all content.

Author Contribution

The authors contributed to this work in different capacities, described as follows. N.L. and E.R. performed cell-based and biochemistry experiments, study design, data acquisition, analysis, and interpretation and wrote the original draft of the manuscript together with A.M.; A.S., M.B. F.B., G.T. and P.F. performed cell-based and biochemistry experiments and participated in the interpretation of the data; M.F-F. and E.P. performed and interpreted the in silico analysis; G.C. and S.B. designed and performed the IHC analysis; L.S. and R.E.B. performed the ex vivo PDX experiments; L.L., I.M., S.B., L.V.

and S.R. developed the methodology, provided administrative and technical support, interpreted the data; E.M., B.S. and R.M.C. generated the PDX models; A.M. conceived, designed, and supervised the study; analyzed and interpreted the data; responsible for funding acquisition, and wrote the original draft of the manuscript together with N.L. All the authors reviewed the prepared manuscript.

References

1. Burstein, H.J., Somerfield, M.R., Barton, D.L., Dorris, A., Fallowfield, L.J., Jain, D., Johnston, S.R.D., Korde, L.A., Litton, J.K., Macrae, E.R., et al. (2021). Endocrine Treatment and Targeted Therapy for Hormone Receptor-Positive, Human Epidermal Growth Factor Receptor 2-Negative Metastatic Breast Cancer: ASCO Guideline Update. J. Clin. Oncol. Off. J. Am. Soc. Clin. Oncol. *39*, 3959–3977. https://doi.org/10.1200/JCO.21.01392.
2. O'Sullivan, C.C., Clarke, R., Goetz, M.P., and Robertson, J. (2023). Cyclin-Dependent Kinase 4/6 Inhibitors for Treatment of Hormone Receptor-Positive, ERBB2-Negative Breast Cancer: A Review. JAMA Oncol. *9*, 1273–1282. https://doi.org/10.1001/jamaoncol.2023.2000.
3. Álvarez-Fernández, M., and Malumbres, M. (2020). Mechanisms of Sensitivity and Resistance to CDK4/6 Inhibition. Cancer Cell *37*, 514–529. https://doi.org/10.1016/j.ccell.2020.03.010.
4. Wander, S.A., Cohen, O., Gong, X., Johnson, G.N., Buendia-Buendia, J.E., Lloyd, M.R., Kim, D., Luo, F., Mao, P., Helvie, K., et al. (2020). The Genomic Landscape of Intrinsic and Acquired Resistance to Cyclin-Dependent Kinase 4/6 Inhibitors in Patients with Hormone Receptor-Positive Metastatic Breast Cancer. Cancer Discov. *10*, 1174–1193. https://doi.org/10.1158/2159-8290.CD-19-1390.
5. Hydbring, P., Malumbres, M., and Sicinski, P. (2016). Non-canonical functions of cell cycle cyclins and cyclin-dependent kinases. Nat. Rev. Mol. Cell Biol. *17*, 280–292. https://doi.org/10.1038/nrm.2016.27.
6. Scheiblecker, L., Klampfl, T., Doma, E., Nebenfuehr, S., Torres-Quesada, O., Strich, S., Heller, G., Werdenich, D., Tschulenk, W., Zojer, M., et al. (2025). CDK6 kinase inhibition unmasks metabolic dependencies in BCR::ABL1 + leukemia. Cell Death Dis. *16*, 107. https://doi.org/10.1038/s41419-025-07434-1.
7. Ziegler, D.V., Parashar, K., and Fajas, L. (2024). Beyond cell cycle regulation: The pleiotropic function of CDK4 in cancer. Semin. Cancer Biol. *98*, 51–63. https://doi.org/10.1016/j.semcancer.2023.12.002.
8. Franco, J., Balaji, U., Freinkman, E., Witkiewicz, A.K., and Knudsen, E.S. (2016). Metabolic Reprogramming of Pancreatic Cancer Mediated by CDK4/6 Inhibition Elicits Unique Vulnerabilities. Cell Rep. *14*, 979–990. https://doi.org/10.1016/j.celrep.2015.12.094.
9. Uzhachenko, R.V., Bharti, V., Ouyang, Z., Blevins, A., Mont, S., Saleh, N., Lawrence, H.A., Shen, C., Chen, S.-C., Ayers, G.D., et al. (2021). Metabolic modulation by CDK4/6 inhibitor promotes chemokine-mediated recruitment of T cells into mammary tumors. Cell Rep. *35*, 108944. https://doi.org/10.1016/j.celrep.2021.108944.

10. Tarrado-Castellarnau, M., Foguet, C., Tarragó-Celada, J., Palobart, M., Hernández-Carro, C., Perarnau, J., Zodda, E., Polat, I.H., Marin, S., Suarez-Bonnet, A., et al. (2025). Glutaminase as a metabolic target of choice to counter acquired resistance to Palbociclib by colorectal cancer cells. Oncogene *44*, 3386–3406. https://doi.org/10.1038/s41388-025-03495-w.
11. Feng, W.W., and Kurokawa, M. (2020). Lipid metabolic reprogramming as an emerging mechanism of resistance to kinase inhibitors in breast cancer. Cancer Drug Resist. *3*, 1–17. https://doi.org/10.20517/cdr.2019.100.
12. Lorito, N., Bacci, M., Smiriglia, A., Mannelli, M., Parri, M., Comito, G., Ippolito, L., Giannoni, E., Bonechi, M., Benelli, M., et al. (2020). Glucose Metabolic Reprogramming of ER Breast Cancer in Acquired Resistance to the CDK4/6 Inhibitor Palbociclib. Cells *9*, 668. https://doi.org/10.3390/cells9030668.
13. Li, X., Sun, Z., Zeng, R., Liu, R., Lin, P., Xing, Z., Jin, X., and Yang, T. (2025). Diet-metabolism-transcription axis modulates the sensitivity to CDK4/6 inhibitors through RB1 in prostate cancer. Cell Rep. *44*, 116530. https://doi.org/10.1016/j.celrep.2025.116530.
14. Herrera-Abreu, M.T., Guan, J., Khalid, U., Ning, J., Costa, M.R., Chan, J., Li, Q., Fortin, J.-P., Wong, W.R., Perampalam, P., et al. (2024). Inhibition of GPX4 enhances CDK4/6 inhibitor and endocrine therapy activity in breast cancer. Nat. Commun. *15*, 9550. https://doi.org/10.1038/s41467-024-53837-7.
15. Hisano, Y., and Hla, T. (2019). Bioactive lysolipids in cancer and angiogenesis. Pharmacol. Ther. *193*, 91–98. https://doi.org/10.1016/j.pharmthera.2018.07.006.
16. Saito, R. de F., Andrade, L.N. de S., Bustos, S.O., and Chammas, R. (2022). Phosphatidylcholine-Derived Lipid Mediators: The Crosstalk Between Cancer Cells and Immune Cells. Front. Immunol. *13*, 768606. https://doi.org/10.3389/fimmu.2022.768606.
17. Jin, W., Broedl, U.C., Monajemi, H., Glick, J.M., and Rader, D.J. (2002). Lipase H, a new member of the triglyceride lipase family synthesized by the intestine. Genomics *80*, 268–273. https://doi.org/10.1006/geno.2002.6837.
18. Yung, Y.C., Stoddard, N.C., and Chun, J. (2014). LPA receptor signaling: pharmacology, physiology, and pathophysiology. J. Lipid Res. *55*, 1192–1214. https://doi.org/10.1194/jlr.R046458.
19. Su, S.-C., Hu, X., Kenney, P.A., Merrill, M.M., Babaian, K.N., Zhang, X.-Y., Maity, T., Yang, S.-F., Lin, X., and Wood, C.G. (2013). Autotaxin-lysophosphatidic acid signaling axis mediates tumorigenesis and development of acquired resistance to sunitinib in renal cell carcinoma. Clin. Cancer Res. Off. J. Am. Assoc. Cancer Res. *19*, 6461–6472. https://doi.org/10.1158/1078-0432.CCR-13-1284.
20. Benesch, M.G.K., Wu, R., Tang, X., Brindley, D.N., Ishikawa, T., and Takabe, K. (2023). Lysophosphatidic Acid Receptor Signaling in the Human Breast Cancer Tumor Microenvironment Elicits Receptor-Dependent Effects on Tumor Progression. Int. J. Mol. Sci. *24*, 9812. https://doi.org/10.3390/ijms24129812.
21. Panupinthu, N., Lee, H.Y., and Mills, G.B. (2010). Lysophosphatidic acid production and action: critical new players in breast cancer initiation and progression. Br. J. Cancer *102*, 941–946. https://doi.org/10.1038/sj.bjc.6605588.

22. Marshall, J.-C.A., Collins, J.W., Nakayama, J., Horak, C.E., Liewehr, D.J., Steinberg, S.M., Albaugh, M., Vidal-Vanaclocha, F., Palmieri, D., Barbier, M., et al. (2012). Effect of inhibition of the lysophosphatidic acid receptor 1 on metastasis and metastatic dormancy in breast cancer. J. Natl. Cancer Inst. *104*, 1306–1319. https://doi.org/10.1093/jnci/djs319.

23. Possemato, R., Marks, K.M., Shaul, Y.D., Pacold, M.E., Kim, D., Birsoy, K., Sethumadhavan, S., Woo, H.-K., Jang, H.G., Jha, A.K., et al. (2011). Functional genomics reveal that the serine synthesis pathway is essential in breast cancer. Nature *476*, 346–350. https://doi.org/10.1038/nature10350.

24. Li, W., Xu, H., Xiao, T., Cong, L., Love, M.I., Zhang, F., Irizarry, R.A., Liu, J.S., Brown, M., and Liu, X.S. (2014). MAGeCK enables robust identification of essential genes from genome-scale CRISPR/Cas9 knockout screens. Genome Biol. *15*, 554. https://doi.org/10.1186/s13059-014-0554-4.

25. Palafox, M., Monserrat, L., Bellet, M., Villacampa, G., Gonzalez-Perez, A., Oliveira, M., Brasó-Maristany, F., Ibrahimi, N., Kannan, S., Mina, L., et al. (2022). High p16 expression and heterozygous RB1 loss are biomarkers for CDK4/6 inhibitor resistance in ER+ breast cancer. Nat. Commun. *13*, 5258. https://doi.org/10.1038/s41467-022-32828-6.

26. Geraldo, L.H.M., Spohr, T.C.L. de S., Amaral, R.F. do, Fonseca, A.C.C. da, Garcia, C., Mendes, F. de A., Freitas, C., dosSantos, M.F., and Lima, F.R.S. (2021). Role of lysophosphatidic acid and its receptors in health and disease: novel therapeutic strategies. Signal Transduct. Target. Ther. *6*, 45. https://doi.org/10.1038/s41392-020-00367-5.

27. Hauck, T., Kadam, S., Heinz, K., Garcia Peraza, M., Schmid, R., Kremer, A.E., Wolf, K., Bauer, A., Horch, R.E., Arkudas, A., et al. (2022). Influence of the autotaxin-lysophosphatidic acid axis on cellular function and cytokine expression in different breast cancer cell lines. Sci. Rep. *12*, 5565. https://doi.org/10.1038/s41598-022-09565-3.

28. Terry, A.R., Nogueira, V., Rho, H., Ramakrishnan, G., Li, J., Kang, S., Pathmasiri, K.C., Bhat, S.A., Jiang, L., Kuchay, S., et al. (2023). CD36 maintains lipid homeostasis via selective uptake of monounsaturated fatty acids during matrix detachment and tumor progression. Cell Metab. *35*, 2060–2076.e9. https://doi.org/10.1016/j.cmet.2023.09.012.

29. Liang, Y., Han, H., Liu, L., Duan, Y., Yang, X., Ma, C., Zhu, Y., Han, J., Li, X., and Chen, Y. (2018). CD36 plays a critical role in proliferation, migration and tamoxifen-inhibited growth of ER-positive breast cancer cells. Oncogenesis *7*, 98. https://doi.org/10.1038/s41389-018-0107-x.

30. Sun, J., Su, Y., Xu, Y., Qin, D., He, Q., Qiu, H., Zhuo, J., and Li, W. (2022). CD36 deficiency inhibits proliferation by cell cycle control in skeletal muscle cells. Front. Physiol. *13*, 947325. https://doi.org/10.3389/fphys.2022.947325.

31. Kuda, O., Pietka, T.A., Demianova, Z., Kudova, E., Cvacka, J., Kopecky, J., and Abumrad, N.A. (2013). Sulfo-N-succinimidyl oleate (SSO) inhibits fatty acid uptake and signaling for intracellular calcium via binding CD36 lysine 164: SSO also inhibits oxidized low density lipoprotein uptake by macrophages. J. Biol. Chem. *288*, 15547–15555. https://doi.org/10.1074/jbc.M113.473298.

32. Malumbres, M., and Barbacid, M. (2009). Cell cycle, CDKs and cancer: a changing paradigm. Nat. Rev. Cancer *9*, 153–166. https://doi.org/10.1038/nrc2602.

33. Sakaue-Sawano, A., Kurokawa, H., Morimura, T., Hanyu, A., Hama, H., Osawa, H., Kashiwagi, S., Fukami, K., Miyata, T., Miyoshi, H., et al. (2008). Visualizing spatiotemporal dynamics of multicellular cell-cycle progression. Cell *132*, 487–498. https://doi.org/10.1016/j.cell.2007.12.033.

34. Gañez-Zapater, A., Kourtis, S., Elbæk, C.R., Espinar, L., Toro-Márquez, C., Coll-Manzano, A., Smiriglia, A., García-López, L., Wiegand, L., Guirola, M., et al. (2026). Cell Cycle Control of Nuclear Metabolism Couples Phosphatidylinositol Signaling to Histone Methylation. Adv. Sci., e01083. https://doi.org/10.1002/advs.202501083.

35. Rugo, H.S., Layman, R.M., Lynce, F., Liu, X., Li, B., McRoy, L., Cohen, A.B., Estevez, M., Curigliano, G., and Brufsky, A. (2025). Real-world progression-free survival of CDK4/6 inhibitors plus an aromatase inhibitor in HR-positive/HER2-negative metastatic breast cancer in United States routine clinical practice. ESMO Open *10*, 105570. https://doi.org/10.1016/j.esmoop.2025.105570.

36. Asciolla, J.J., Wu, X., Adamopoulos, C., Gavathiotis, E., and Poulikakos, P.I. (2025). Resistance mechanisms and therapeutic strategies of CDK4 and CDK6 kinase targeting in cancer. Nat. Cancer *6*, 24–40. https://doi.org/10.1038/s43018-024-00893-z.

37. Bacci, M., Lorito, N., Smiriglia, A., Subbiani, A., Bonechi, F., Comito, G., Morriset, L., El Botty, R., Benelli, M., López-Velazco, J.I., et al. (2024). Acetyl-CoA carboxylase 1 controls a lipid droplet-peroxisome axis and is a vulnerability of endocrine-resistant ER+ breast cancer. Sci. Transl. Med. *16*, eadf9874. https://doi.org/10.1126/scitranslmed.adf9874.

38. Du, T., Sikora, M.J., Levine, K.M., Tasdemir, N., Riggins, R.B., Wendell, S.G., Van Houten, B., and Oesterreich, S. (2018). Key regulators of lipid metabolism drive endocrine resistance in invasive lobular breast cancer. Breast Cancer Res. BCR *20*, 106. https://doi.org/10.1186/s13058-018-1041-8.

39. Ward, A.V., Riley, D., Cosper, K.E., Finlay-Schultz, J., Brechbuhl, H.M., Libby, A.E., Hill, K.B., Varshney, R.R., Kabos, P., Rudolph, M.C., et al. (2025). Lipid metabolic reprogramming drives triglyceride storage and variable sensitivity to FASN inhibition in endocrine-resistant breast cancer cells. Breast Cancer Res. BCR *27*, 32. https://doi.org/10.1186/s13058-025-01991-1.

40. Han, L., Jiang, Y., Shi, M., Gan, L., Wu, Z., Xue, M., Zhu, Y., Xiong, C., Wang, T., Lin, X., et al. (2023). LIPH contributes to glycolytic phenotype in pancreatic ductal adenocarcinoma by activating LPA/LPAR axis and maintaining ALDOA stability. J. Transl. Med. *21*, 838. https://doi.org/10.1186/s12967-023-04702-6.

41. Takai, M., Yamamoto, M., Yashiro, N., and Tsujiuchi, T. (2024). Involvement of lysophosphatidic acid (LPA) receptor-mediated signaling in breast cancer cell functions by long-term tamoxifen treatment under hypoxic and estrogen-deprived conditions. Pathol. Res. Pract. *260*, 155385. https://doi.org/10.1016/j.prp.2024.155385.

42. Silverstein, R.L., and Febbraio, M. (2009). CD36, a scavenger receptor involved in immunity, metabolism, angiogenesis, and behavior. Sci. Signal. *2*, re3. https://doi.org/10.1126/scisignal.272re3.

43. Pascual, G., Avgustinova, A., Mejetta, S., Martín, M., Castellanos, A., Attolini, C.S.-O., Berenguer, A., Prats, N., Toll, A., Hueto, J.A., et al. (2017). Targeting metastasis-initiating cells through the fatty acid

receptor CD36. Nature *541*, 41–45. https://doi.org/10.1038/nature20791.

44. Wang, J., and Li, Y. (2019). CD36 tango in cancer: signaling pathways and functions. Theranostics *9*, 4893–4908. https://doi.org/10.7150/thno.36037.
45. Wagner, V., and Gil, J. (2020). Senescence as a therapeutically relevant response to CDK4/6 inhibitors. Oncogene *39*, 5165–5176. https://doi.org/10.1038/s41388-020-1354-9.
46. Yamamoto, M., Takai, M., Yashiro, N., Taniguchi, A., Tamura, M., Kusumoto, Y., Nagano, S., and Tsujiuchi, T. (2024). The role of LPA receptor signaling in modulating cellular responses of colon cancer cells co-cultured with lymphoid endothelial cells under hypoxic stress. Tissue Cell *91*, 102528. https://doi.org/10.1016/j.tice.2024.102528.
47. Bacci, M., Lorito, N., Ippolito, L., Ramazzotti, M., Luti, S., Romagnoli, S., Parri, M., Bianchini, F., Cappellesso, F., Virga, F., et al. (2019). Reprogramming of Amino Acid Transporters to Support Aspartate and Glutamate Dependency Sustains Endocrine Resistance in Breast Cancer. Cell Rep. *28*, 104–118.e8. https://doi.org/10.1016/j.celrep.2019.06.010.
48. Wang, B., Wang, M., Zhang, W., Xiao, T., Chen, C.-H., Wu, A., Wu, F., Traugh, N., Wang, X., Li, Z., et al. (2019). Integrative analysis of pooled CRISPR genetic screens using MAGeCKFlute. Nat. Protoc. *14*, 756–780. https://doi.org/10.1038/s41596-018-0113-7.
49. Simões, B.M., O'Brien, C.S., Eyre, R., Silva, A., Yu, L., Sarmiento-Castro, A., Alférez, D.G., Spence, K., Santiago-Gómez, A., Chemi, F., et al. (2015). Anti-estrogen Resistance in Human Breast Tumors Is Driven by JAG1-NOTCH4-Dependent Cancer Stem Cell Activity. Cell Rep. *12*, 1968–1977. https://doi.org/10.1016/j.celrep.2015.08.050.
50. Montaudon, E., Nikitorowicz-Buniak, J., Sourd, L., Morisset, L., El Botty, R., Huguet, L., Dahmani, A., Painsec, P., Nemati, F., Vacher, S., et al. (2020). PLK1 inhibition exhibits strong anti-tumoral activity in CCND1-driven breast cancer metastases with acquired palbociclib resistance. Nat. Commun. *11*, 4053. https://doi.org/10.1038/s41467-020-17697-1.
51. Soosainathan, A., Iravani, M., El-Botty, R., Alexander, J., Sourd, L., Morisset, L., Painsec, P., Orha, R., Nikitorowicz-Buniak, J., Pancholi, S., et al. (2024). Targeting Transcriptional Regulation with a CDK9 Inhibitor Suppresses Growth of Endocrine- and Palbociclib-Resistant ER+ Breast Cancers. Cancer Res. *84*, 17–25. https://doi.org/10.1158/0008-5472.CAN-23-0650.
52. Pereira, B., Chin, S.-F., Rueda, O.M., Vollan, H.-K.M., Provenzano, E., Bardwell, H.A., Pugh, M., Jones, L., Russell, R., Sammut, S.-J., et al. (2016). The somatic mutation profiles of 2,433 breast cancers refines their genomic and transcriptomic landscapes. Nat. Commun. *7*, 11479. https://doi.org/10.1038/ncomms11479.

Figures

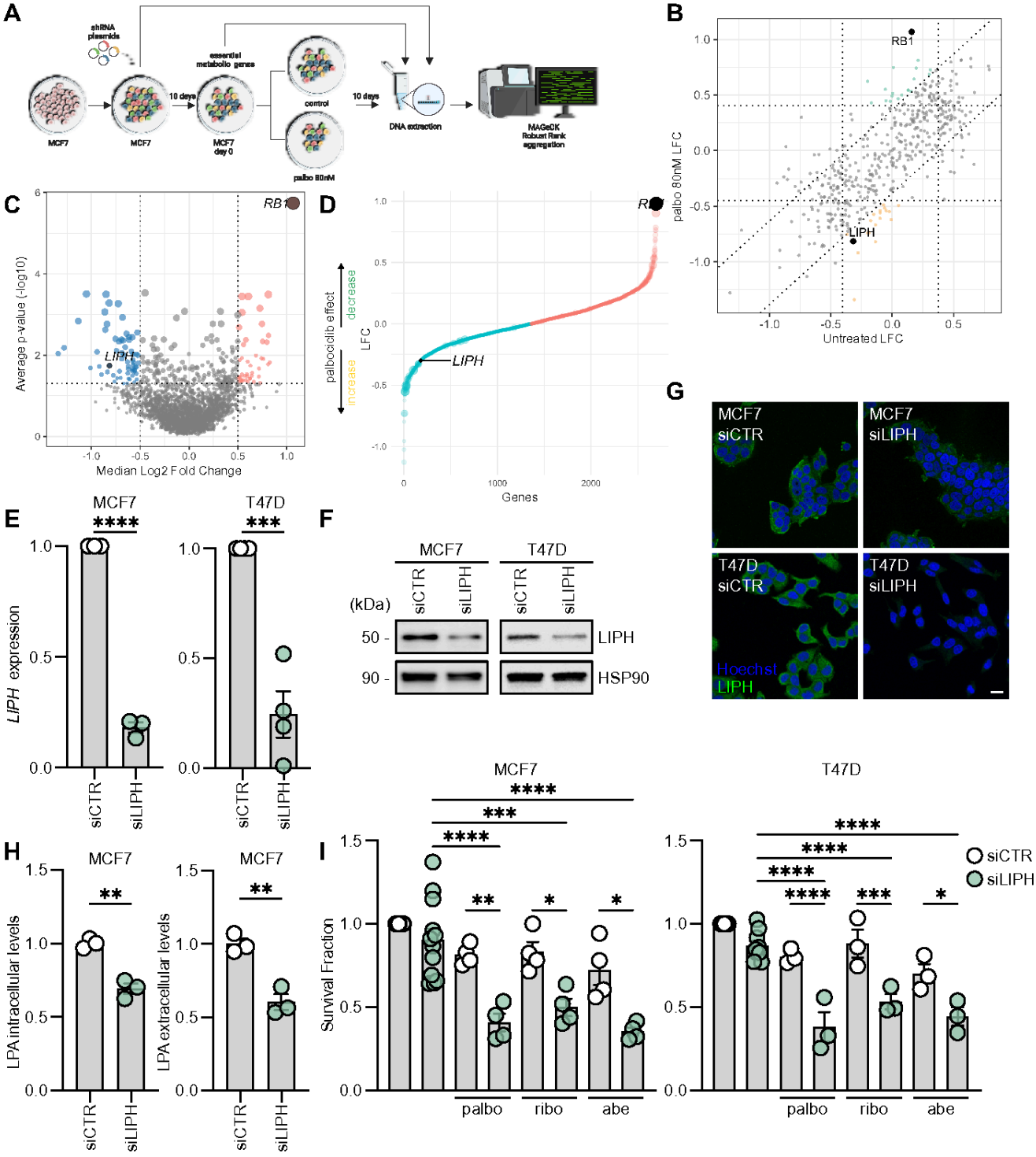


Figure 1

Figure 1

A metabolic dropout screen identifies LIPH as a regulator of CDK4/6i sensitivity. (A) Schematic outline of the pooled shRNA loss-of-function screen performed in MCF7 cells. Cells were infected with a metabolism-focused shRNA library targeting 2,752 metabolic genes and cultured for 10 days. Genomic DNA isolated from surviving cells was used as baseline reference population (MCF7 Day 0). In parallel, infected cells were treated for an additional 10 days with 80 nM palbociclib (palbo, IC20 concentration),

and shRNA abundance was quantified by next-generation sequencing followed by MAGeCK analysis. (B) Nine-square plot showing log fold change (LFC) values when compared to Day 0 of the untreated (x-axis) and palbociclib-treated (y-axis) populations. Cutoffs correspond to ±1.5*SD of each population, and only genes with >2 shRNAs and p-value < 0.05 are shown. Bottom center quadrant contains dropout shRNAs targeting genes highlighted in orange; the upper center quadrant shows enriched shRNAs targeting genes highlighted in green. (C) Volcano plot showing genes enriched or depleted following palbociclib treatment relative to baseline conditions (Day 0). (D) Rank plot (MCF7 - Day 0) of candidate modulator genes identified in the screen. LFC distribution highlighted *RB1* and *LIPH*among the top candidate desensitizers and sensitizers, respectively, of palbociclib response. (E) MCF7 and T47D cells were transfected with control (siCTR) or LIPH-targeting siRNA (siLIPH) for 48 hours and subjected to qRT-PCR analysis to assess LIPH mRNA expression. Fold relative enrichment is represented relative to siCTR-transfected cells. (F, G) MCF7 and T47D cells were transfected with siCTR or siLIPH for 48 hours and analyzed by western blotting (F) and immunofluorescence (G) to assess LIPH protein level. Representative images are shown. Green, LIPH; blue, Hoechst (nuclei). Scale bars, 25 μm. (H) Intracellular and extracellular LPA levels were measured in MCF7 cells 48 hours after transfection with siCTR or siLIPH. Fold relative enrichment is represented relative to siCTR-transfected cells. (I) MCF7 and T47D cells were transfected with siCTR or siLIPH and subsequently treated with palbo (40 nM), ribociclib (ribo, 50 nM), or abemaciclib (abe, 20 nM) for 10 days before cell counting. Survival fractions are represented relative to untreated to siCTR-transfected cells. Data are mean ± SEM. Each dot represents a replicate from at least three independent biological experiments. Statistical analysis was performed using two-tailed unpaired Student’s t-test (E, H) or one-way ANOVA with Tukey’s multiple comparisons test (I). *P < 0.05; **P < 0.01; ***P < 0.001; ****P < 0.0001.

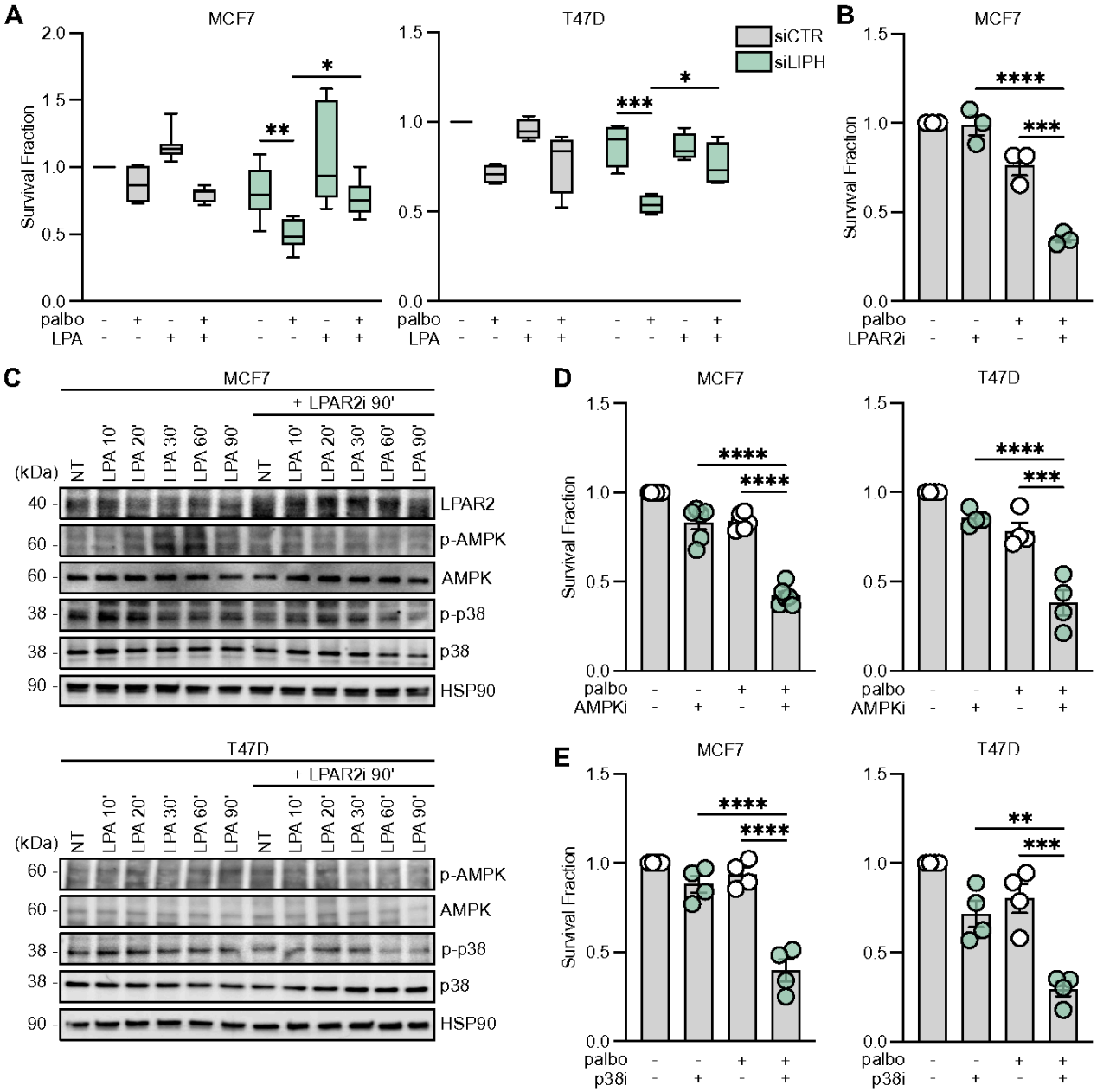


Figure 2

Figure 2

LPA-LPAR2 signaling facilitates the sensitization to CDK4/6i. (A) MCF7 and T47D cells were transfected with siCTR or siLIPH and subsequently treated with palbo (40 nM) in the presence or absence of exogenous LPA (10 μM) for 10 days (MCF7) or with palbo (80 nM) in the presence or absence of exogenous LPA (15 μM) for 3 days (T47D) before cell counting. Survival fractions are represented relative to untreated control cells. (B) MCF7 and T47D cells were stimulated with LPA (20 μM) and, where

indicated, cells were pre-treated with an LPAR2 inhibitor (LPAR2i, 50 μM) before LPA administration, for the indicated times, and subjected to western blotting analysis using the antibodies indicated. (C) MCF7 cells were treated with palbo (40 nM), the LPAR2i (25 μM), or the combination for 10 days before cell counting. Survival fraction is represented relative to untreated cells. (D, E) MCF7 and T47D cells were treated with palbo (40 nM) in combination with an AMPK inhibitor (AMPKi, 2.5 μM) or a p38 inhibitor (p38i, 5 μM) for 10 days before cell counting. Data are mean ± SEM. Each dot represents a replicate from at least three independent biological experiments. Statistical analysis was performed using two-way ANOVA with Šidák's multiple comparisons test (A) or one-way ANOVA with Tukey's multiple comparisons test (C, D, E). *P < 0.05; **P < 0.01; ***P < 0.001; ****P < 0.0001.

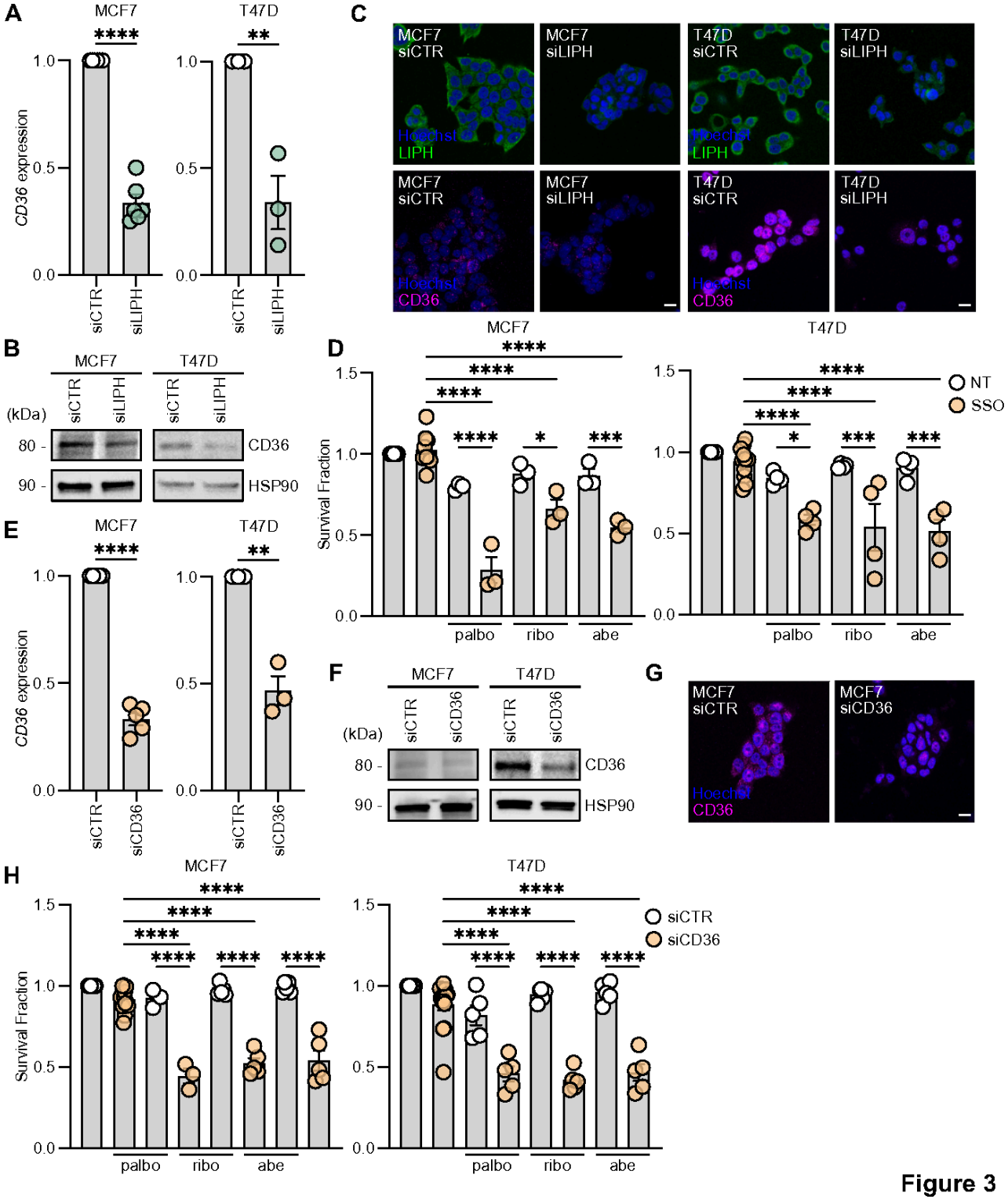


Figure 3

Figure 3

CD36 links LPA signaling to CDK4/6 inhibitor response. (A) MCF7 and T47D cells were transfected with siCTR or siLIPH for 48 hours and subjected to qRT-PCR analysis to assess CD36 mRNA expression. Fold relative enrichment is represented relative to siCTR-transfected cells. (B, C) MCF7 and T47D cells were transfected with siCTR or siLIPH for 48 hours and subjected to western blotting (B) or immunofluorescence (C) analysis to evaluate CD36 protein level. Representative images are shown.

Green, LIPH; pink, CD36; blue, Hoechst (nuclei). Scale bars, 25 μm. (D) MCF7 and T47D cells were treated with palbo (40 nM), ribo (50 nM), or abe (20 nM) in the presence or absence of the CD36 inhibitor SSO (10 μM) for 10 days before cell counting. Survival fractions are represented relative to untreated cells. (E) MCF7 and T47D cells were transfected with siCTR or CD36-targeting siRNA (siCD36) for 48 hours and subjected to qRT-PCR analysis to assess CD36 mRNA expression. Fold relative enrichment is represented relative to siCTR-transfected cells. (F, G) MCF7 and T47D cells were transfected with siCTR or siCD36 for 48 hours and subjected to western blot analysis (F) or immunofluorescence (G) analysis to confirm CD36 depletion. Representative images are shown. Pink, CD36; blue, Hoechst (nuclei). Scale bars, 25 μm. (H) MCF7 and T47D cells were transfected with siCTR or siCD36 and subsequently treated with palbo (40 nM), ribo (50 nM), or abe (20 nM) for 10 days before cell counting. Survival fractions are represented relative to untreated siCTR-transfected cells. Data are mean ± SEM. Each dot represents a replicate from at least three independent biological experiments. Statistical analysis was performed using two-tailed unpaired Student's t-test (A, E) or one-way ANOVA with Tukey's multiple comparisons test (D, H). *P < 0.05; **P < 0.01; ***P < 0.001; ****P < 0.0001.

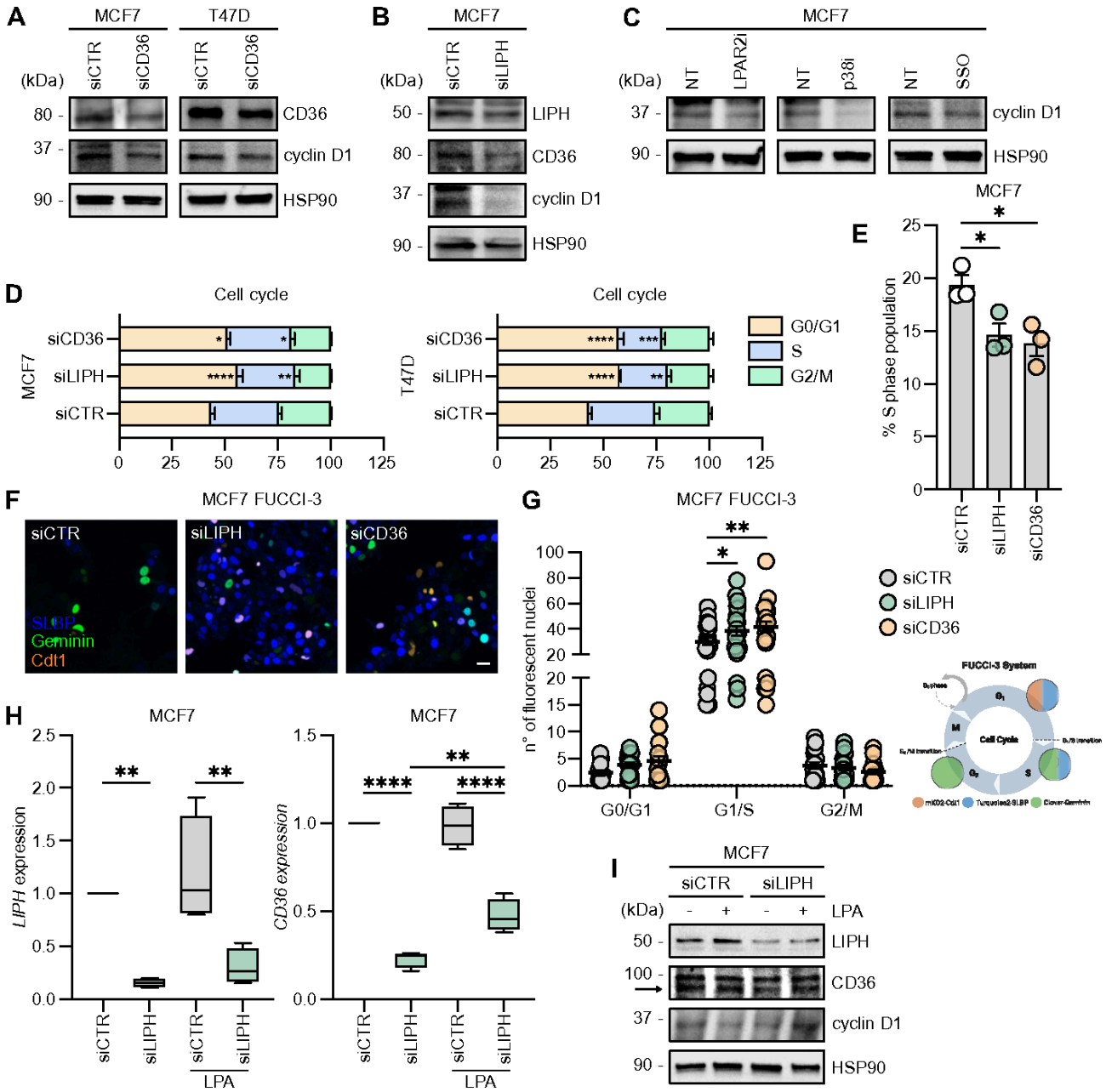


Figure 4

Figure 4

The LIPH-LPA-CD36 signaling axis regulates cyclin D1 expression and cell cycle progression. (A) MCF7 and T47D cells were transfected with siCTR or siCD36 for 48 hours and subjected to western blotting analysis using the antibodies indicated. (B) MCF7 cells were transfected with siCTR or siLIPH for 48 hours and subjected to western blotting analysis using the antibodies indicated. (C) MCF7 cells were treated with the LPAR2i (50 μM), p38i (15 μM), or the CD36 inhibitor SSO (20 μM) for 24 hours and

subjected to western blotting to assess cyclin D1 protein expression. (D, E) MCF7 and T47D cells were transfected with siCTR, siLIPH, or siCD36 for 48 hours and subjected to propidium iodide (PI, D) and 5-ethynyl-2´-deoxyuridine (EdU)-based (E) flow cytometric cell cycle analysis. Representative cell cycle phase distributions (D) and quantification of S phase population (E) are shown. (F, G) MCF7 FUCCI-3 cells were transfected with siCTR, siLIPH, or siCD36 for 48 hours and analyzed by confocal microscopy. Representative images of MCF7 FUCCI-3 cells are shown in (F), and quantification of cell cycle phase distribution is shown in (G). The G0/G1 phase is characterized by high Cdt1-mKO2 (orange) expression together with low Clover-Geminin (green) and increased SLBP-Turquoise2 (blue) levels. Cells in the G1/S transition display enhanced Clover-Geminin expression, whereas cells progressing through G2/M exhibit the highest levels of Clover-Geminin, and a progressive loss of SLBP-Turquoise2 and Cdt1-mKO2 expression. Scale bars, 25 μm. (H, I) MCF7 cells were transfected with siCTR or siLIPH and subsequently treated with exogenous LPA (15 μM) for 48 hours before qRT-PCR (H) and western blotting (I) analysis using the antibodies indicated. Fold relative enrichment is represented relative to untreated siCTR-transfected cells. Data are mean ± SEM. Each dot represents a replicate from at least three independent biological experiments. Statistical analysis was performed using two-way ANOVA with Tukey's multiple comparisons test (D, G) or one-way ANOVA with Tukey's multiple comparisons test (E, H). *P < 0.05; **P < 0.01; ***P < 0.001; ****P < 0.0001.

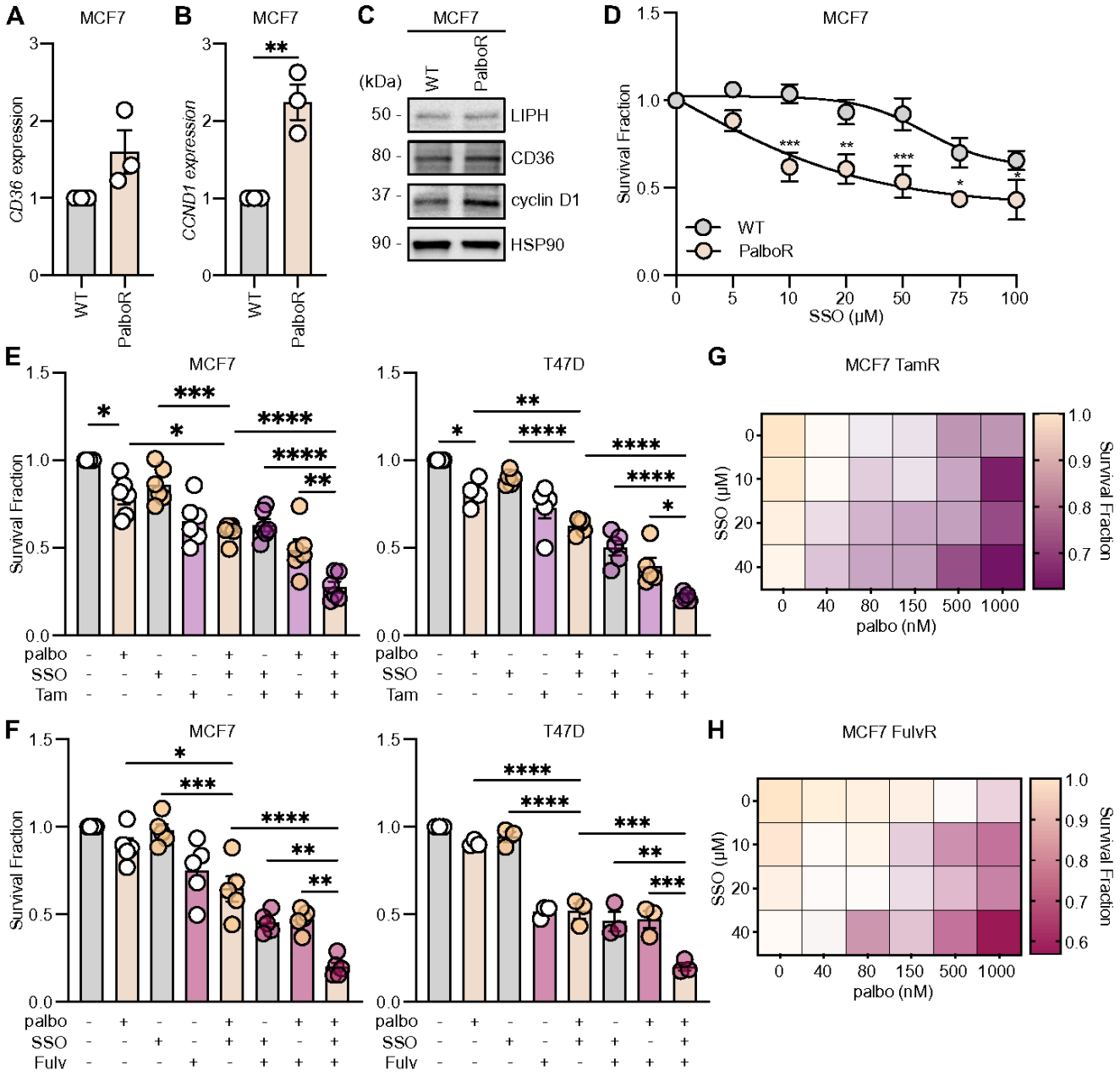


Figure 5

Figure 5

CD36 targeting sensitizes resistant ER+ breast cancer cells. (A, B) MCF7 wild-type cells (WT) and palbociclib-resistant derivatives (PalboR) were subjected to ddPCR analysis to assess CD36 and CCND1 mRNA expression. Fold relative enrichment is represented relative to MCF7 WT cells. (C) WT and PalboR MCF7 cells were subjected to western blotting analysis using the antibodies indicated. (D) WT and PalboR MCF7 cells were treated with increasing concentrations of the CD36 inhibitor SSO for 72 hours

and subjected to cell counting. Dose-response curves are shown. (E, F) MCF7 and T47D cells were treated with palbo (40 nM), SSO (10 μM), tamoxifen (Tam, 500 nM, E), or fulvestrant (Fulv, 50 nM, F), as single agents or in the indicated combinations, for 10 days before cell counting. Survival fractions are represented relative to untreated cells. (G, H) Tamoxifen-resistant (TamR) and fulvestrant-resistant (FulvR) MCF7 derivatives were treated with the indicated increasing doses of palbo and SSO, alone or in combination, for 3 days before the crystal violet assay. Heatmaps represent relative cell survival normalized to untreated cells. Data are mean ± SEM. Each dot represents a replicate from at least three independent biological experiments. Statistical analysis was performed using two-tailed unpaired Student's t-test (A, B), two-way ANOVA with Tukey's multiple comparisons test (D) or one-way ANOVA with Tukey's multiple comparisons test (E, F). *P < 0.05; **P < 0.01; ***P < 0.001; ****P < 0.0001.

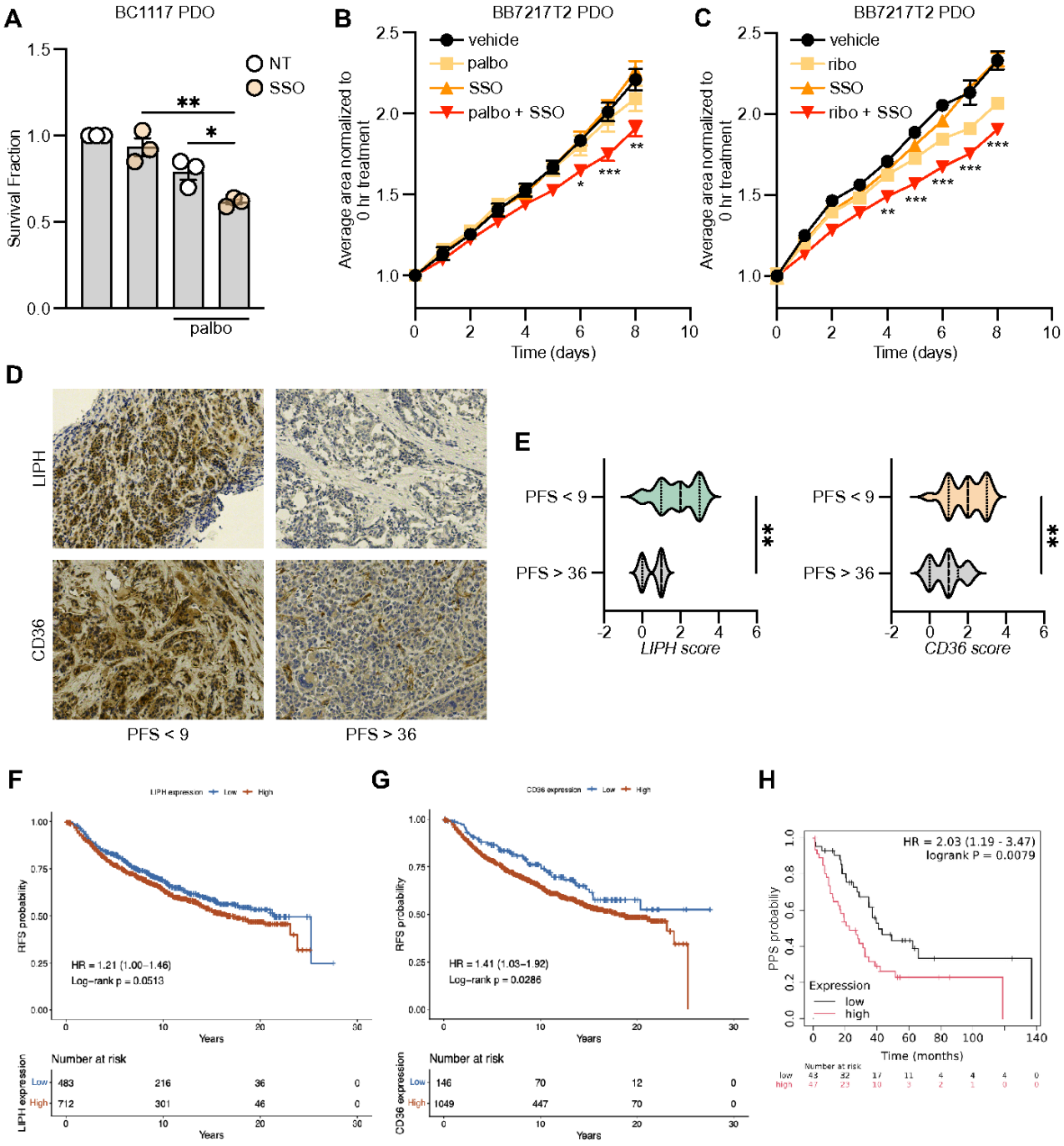


Figure 6

Figure 6

The LIPH-CD36 axis correlates with clinical outcome in ER+ breast cancer.

(A) The ER+ breast cancer PDO HBCx-139-org was treated with palbo (0.3 μM), the CD36 inhibitor SSO (0.3 μM), or the combination and monitored using the CellTiter-Glo® 3D Cell Viability Assay. Survival fractions are represented relative to the vehicle. (B, C) The ER+ breast cancer PDO BB7217T2 was

treated with palbo (1 μM) or ribo (500 nM), alone or in combination with SSO (50-25 μM, respectively), and monitored using live-cell imaging. Organoid growth was quantified over time using Incucyte analysis software. (D, E) IHC staining of LIPH and CD36 in tumor samples obtained from patients with ER+/HER2− breast cancer treated with CDK4/6i-based therapy. Patients were stratified according to PFS, with poor responders defined as PFS < 9 months and long responders defined as PFS > 36 months. Representative 20X images and scores are shown. Scale bars, 200 μm. (F, G) Kaplan-Meier analyses of LIPH and CD36 in ER+/HER2- patients from the METABRIC cohort. Patients were stratified into high and low expression groups as described in Materials and Methods. Hazard ratios and log-rank p-values are indicated in the panels. (H) Kaplan-Meier analyses of PPS according to the combined LIPH/LPAR2/CD36 expression signature in a curated cohort of ER+/HER2- patients. Patients were stratified into high and low expression groups as described in Materials and Methods. Hazard ratios and log-rank p-values are indicated in the panels. Data are mean ± SEM. Each dot represents a replicate from at least three independent biological experiments. Statistical analysis was performed using one-way ANOVA with Tukey's multiple comparisons test (A), two-way ANOVA with Dunnett's multiple comparisons test (B, C) or two-tailed unpaired Student's t-test (E). *P < 0.05; **P < 0.01; ***P < 0.001.

Supplementary Files

This is a list of supplementary files associated with this preprint. Click to download.

- Figure1S.pdf
- Figure2S.pdf
- Figure3S.pdf
- Graphicalabstract.docx